# Cholesterol binding to the transmembrane region of a group 2 HA of Influenza virus is essential for virus replication affecting both virus assembly and HA´s fusion activity

**Bodan Hu**[a], **Chris Tina Höfer**[a], **Christoph Thiele**[b], **Michael Veit**[a] #

[a] Institut für Virologie, Freie Universität Berlin, Berlin, Germany.

[b] Biochemistry and Cell Biology of Lipids, Life & Medical Sciences Institute (LIMES), University of Bonn, Germany

Running head: Cholesterol binding to HA

#Address correspondence to Michael Veit: mveit@zedat.fu-berlin.de

Word count for the abstract: 248

Word count for the text: 9476

Keywords: Influenza virus; Hemagglutinin; transmembrane region; cholesterol; virus assembly; membrane fusion

**ABSTRACT**

Hemagglutinin (HA) of Influenza virus is incorporated into cholesterol enriched, nanodomains of the plasma membrane. Phylogenetic group 2 HAs contain the conserved cholesterol consensus motif (CCM) YKLW in the transmembrane region. We previously reported that mutations in the CCM retarded intracellular transport of HA and decreased its nanodomain association. Here we analyzed whether cholesterol interacts with the CCM. Incorporation of photocholesterol into HA was significantly reduced if the whole CCM is replaced by alanine, both using immunoprecipitated HA and when HA is embedded in the membrane. Next, we used reverse genetics to investigate the significance of the CCM for virus replication. No virus was rescued if the whole motif is exchanged (YKLW4A); single (LA) or double (YK2A and LW2A) mutated virus showed decreased titers and a comparative fitness disadvantage. In polarized cells transport of HA mutants to the apical membrane was not disturbed. Reduced amounts of HA and cholesterol were incorporated into the viral membrane. Mutant viruses exhibit a decrease in hemolysis, which is only partially corrected if the membrane is replenished with cholesterol. More specifically, viruses have a defect in hemifusion as demonstrated by fluorescence dequenching. Cells expressing HA-YKLW4A fuse with erythrocytes, but the number of events are reduced. Even after acidification unfused erythrocytes remain cell-bound, a phenomenon not observed with wildtype HA. We conclude that cholesterol-binding to a group 2 HA is essential for virus replication. It has pleiotropic effects on virus assembly and membrane fusion, mainly on lipid mixing and possibly a preceding step.

## IMPORTANCE

The glycoprotein hemagglutinin (HA) is a major pathogenicity factor of Influenza viruses. Whereas the structure and function of HA´s ectodomain is known in great detail, similar data for the membrane-anchoring part of the protein are missing. Here we demonstrate that the transmembrane region of a group 2 HA interacts with cholesterol, the major lipid of the plasma membrane and the defining element of the viral budding site nanodomains of the plama membrane. The cholesterol binding motif is essential for virus replication. Its partial removal affects various steps of the viral life cycle, such as assembly of new virus particles and their subsequent cell entry via membrane fusion. A cholesterol-binding pocket in group 2 HAs might be a promising target for a small lipophilic drug that inactivates the virus.

## INTRODUCTION

Hemagglutinin (HA) of Influenza virus is a typical type I transmembrane glycoprotein with an N-terminal signal peptide, a large ectodomain, a single transmembrane region and a short cytoplasmic tail (1). HA assembles into homotrimers in the ER and is transported via the secretory pathway to the plasma membrane, in polarized cells to the apical membrane, where virus assembly and budding take place (2). It was proposed that Influenza virus assembles in and buds through small dynamic, cholesterol- and sphingolipid-enriched nanodomains of the plasma membrane which could coalesce to larger, more stable platforms (3, 4). Indeed, it was demonstrated by quantitative mass spectrometry that these lipids are enriched in the viral membrane relative to the entire apical membrane of their host cell (5). HA organizes the viral assembly site, since it is not randomly distributed in the plasma membrane of transfected cells, but is present in (partly cholesterol-sensitive) clusters of various sizes as demonstrated by quantitative immunoelectron microscopy (6-8) and FPALM (fluorescence-photoactivation-localization microscopy) (9). The other integral membrane proteins of the virus, the neuraminidase (NA) and the ion channel M2 contain their own signals for targeting to the viral assembly site (10), where they are supposed to recruit the internal components of viral particles, the matrix protein M1 and the eight ribonucleoparticles (containing the viral genome segments complexed to the nucleoprotein (NP) and the three polymerase proteins PA, PB1 and PB2) into budding virions (11, 12).

HA plays also a pivotal role during virus entry. It is responsible for receptor recognition: A binding pocket in the globular head domain of the molecule recognizes sialic acid moieties in glycoproteins and glycolipids on the host cell surface. After clathrin-mediated endocytosis of the virus acidification of the endosome triggers an irreversible conformational change in HA (1). In order to perform the conformational change the inactive precursor HA0 must first be processed into two disulfide-linked subunits, the membrane-embedded HA2 and the globular HA1 subunit, by a protease provided by the host organism (13). The elucidation of the crystal structures of the ectodomain of HA at neutral and a part of the ectodomain at mildly acidic pH has led to a model of how conformational changes of HA execute membrane fusion. The hydrophobic fusion peptide at the N-terminus of HA2, which is buried inside the trimeric structure at neutral pH, becomes exposed on the distal end of the molecule after acidification and interacts with the cellular membrane. A second conformational change then bends the HA-molecule thereby drawing the fusion peptide towards the transmembrane region which leads to close apposition of both lipid bilayers (1). By mechanisms that are not well understood at present lipid exchange initially only occurs between the outer leaflets of the viral and the cellular membrane (hemifusion). Finally, a fusion pore opens, flickers and dilates thereby allowing entry of the viral genome into the target cell (14). Analysing the fusion kinetics of individual virus particles indicated that exposure of the fusion peptide is the rate-limiting step of the reaction. Full fusion then requires the cooperative action of three to four neighbouring HA trimers that pull together on the cellular membrane to execute fusion (15).

The C-terminal membrane anchoring fragment of HA, for which no structure has been elucidated, also contributes to membrane fusion. Fusion pore formation requires the presence of a transmembrane region with a minimal length of 17 amino acids (16); HA anchored to the outer leaflet of the membrane by a glycolipid instead of the TMR may cause hemifusion after acidification, but is not able to catalyze full fusion (17). The cytoplasmic tail plays a role during fusion pore formation; it requires S-acylation at conserved cysteine residues at least in some HA subtypes (18), whereas other (artificial) modifications of the tail negatively affect fusion (19, 20).

The lipids in the membrane destined to fuse are also not passive bystanders of the reaction. Since fusion requires strong bending of the bilayer, certain lipid species with an intrinsic curvature, i.e. those having a small head group and a large tail (or *vice versa*) positively or negatively affect certain stages of the reaction (21). One abundant lipid species with a negative intrinsic curvature is cholesterol, since it consists of a small hydrophilic head group, a large and rigid steroid ring structure and a flexible hydrocarbon tail and thus it may stabilize highly curved fusion intermediates. Indeed, cholesterol addition or removal from the HA-containing membrane positively or negatively affects the extent of fusion (22, 23). Cholesterol acts at two stages in membrane fusion: at an early, lipidic stage prior to fusion pore opening and a later stage during fusion pore expansion (22). However, the mechanism of the effect of cholesterol on fusion is not understood and is probably more complex than stabilizing highly curved lipid intermediates. Cholesterol prevents unphysiological ("leaky") fusion reactions (24), affects membrane ordering (and hence the lateral mobility of

98 HA), the spatial distance of HA in virus particles (25) and finally allows liquid phase
99 separation that concentrates HA for efficient fusion (26).
100 Hemagglutinin has two signals for targeting to cholesterol-enriched nanodomains. On
101 one hand, three conserved S-acylated cysteines located at the cytoplasmic end of the
102 TMR and in the cytoplasmic domain, respectively (27-29), on the other hand,
103 hydrophobic amino acids in the TMR facing the outer leaflet of the plasma
104 membrane, especially the conserved amino acids VIL at the beginning of the TMR.
105 The latter were identified by alanine scanning mutagenesis throughout the whole
106 TMR of HA to identify residues that confer incorporation of HA into
107 detergent-resistant-membranes (DRMs), the biochemical correlate of membrane
108 nanodomains (26, 30). Mutation of these amino acids at the beginning of the TMR
109 also reduced fluorescence resonance energy transfer (FRET) of HA with a
110 double-acylated raft-marker (27, 29, 31).
111 We reported recently that leucine of VIL might be part of a cholesterol consensus
112 motif (CCM) that is known to bind cholesterol to 7-transmembrane-receptors
113 (7TMR). By crystallography the cholesterol-interacting amino acids in the human
114 ß-adrenergic receptor were identified and by sequence comparison with other 7TMR
115 the cholesterol consensus motif (CCM) was defined (32). In the CCM the amino acids
116 interacting with cholesterol are not a linear sequence motif, but distributed between
117 two transmembrane helices of these polytopic membrane proteins. One helix contains
118 the sequence motif W/Y-I/V/L-K/R, whereby all residues must face the same side of
119 the helix. In addition, another aromatic amino acid, either phenylalanine (F) or

tyrosine (Y) is needed on a second helix to bind cholesterol from the other side. Since cholesterol is present in both leaflets of a bilayer (33), the CCM can be orientated in two ways; the charged amino acid might face either the extracellular space or the cytosolic compartment (34-36).

HAs of the phylogenetic group 2 contain a strictly conserved YKLW motif which conforms to the CCM defined for 7TMR (F/Y-R/K-I/V/L-Y/W). Mutations in the CCM drastically retard Golgi-localized processing of HA, such as acquisition of Endo-H resistant carbohydrates in the medial-Golgi and proteolytic cleavage in the TGN. All mutants analysed by FRET also showed reduced association with nanodomains at the plasma membrane (37).

Here we analysed whether the CCM indeed interacts with cholesterol and if mutations in the CCM affect virus replication, virus assembly and membrane fusion.

## MATERIAL AND METHODS

### Cell culture and virus experiments

Madin Darby canine kidney (MDCK II), Chinese hamster ovary (CHO) and human embryonic kidney 293T cells were grown in DMEM (Dulbecco's modification of Eagle's medium, PAN, Aidenbach, Germany) supplemented with 10% FCS (fetal calf serum, Perbio, Bonn, Germany) and penicillin/streptomycin (100 units/ml and 100 µg/ml, respectively) at 37 °C and 5% CO2. To generate polarized cells, $5x10^5$ MDCK II cells were seeded into 24 mm transwells containing a polyester membrane with pores having a diameter of 0.4 µm (Corning) using 1.5 ml growth medium in the upper and 2.6 ml in the lower chamber. Medium was exchanged every day and cells were cultured for 4 days.

Mutant 1 of the highly pathogenic strain A/FPV/Rostock/1934 (H7N1), termed FPV*, that contains the sequence PSKGR instead of PSKKRKKR at the C-terminus of HA1 (38) was used to create recombinant virus. FPV* shows low pathogenicity in chicken and requires trypsin for growth in cell culture and is thus suitable for working in a BSL2 lab. The full-length sequence (excluding the fluorophore) of HA mutants LA, YK2A, LW2A and YKLW4A were cloned from plasmid pECerulean (37) to pHH21 with In-Fusion® HD Cloning Kit (Takara Bio, Japan). Recombinant Influenza viruses were produced with the twelve plasmids system (38) by transfection (0.5 µg of each plasmid) of 293T cells in 35 mm dishes with TurboFect reagent. 4-6 h later, the medium was changed to infection medium (DMEM, 0.1% FCS, 0.2% BSA, 1 µg/ml TPCK-Trypsin). 48 h post transfection, the supernatant was harvested and centrifuged

154 at 2000 g for 5 min to clear from cell debris and further amplified in MDCK II cells to
155 generate a virus stock.
156 HA tests were performed in 96 well U-bottom microwell plates. 50 µl of a two-fold
157 serial dilution of virus sample in PBS was incubated with 50 µl 1% chicken red blood
158 cells for 30 minutes at room temperature.
159 For TCID50 tests virus samples were three-fold serially diluted in infection medium.
160 100 µl diluted virus samples (8 replicates) were added to confluent MDCK II cells in
161 96-well plates after washing the cells once with DPBS+ (Dulbecco's
162 phosphate-buffered saline with Calcium and Magnesium, PAN biotech, Germany). 2
163 days post infection, cells were washed once with PBS, fixed with 3% formaldehyde in
164 PBS for 5 min and stained with 0.1% crystal violet. The TCID50 titer was calculated
165 by Reed & Muench Method.
166 To generate a growth curve, 90% confluent MDCK II cells in 6-well plates were
167 infected with FPV*-wt or mutants with a moi of 0.0005 (based on TCID50 titer). 1 h
168 post infection, medium was replaced by infection medium, aliquots of culture
169 supernatant were harvested at 12 h, 24 h, 36 h and 48 h post infection, cleared from
170 cell debris (2000 g, 5 min) and titrated by TCID50 and HA-assay.
171 For competitive growth experiments FPV* mutant was mixed with wild type at a ratio
172 of 5 to 1 and MDCK II cells were infected with total moi of 0.0005. vRNA was
173 extracted from the virus mixture or at 24 h and 48 h post infection from the cell
174 culture supernatant with RTP® DNA/RNA Virus Mini Kit (Stratec, Germany).
175 OneStep RT-PCR Kit (Qiagen) was used for reverse transcription of HA fragment

with specific primers (Forward: TGAAAATGGTTGGGAAGGTCTGG, Reverse: CGCATGTTTCCGTTCTTCACAC), which were then sent for sequencing.

For growth experiments in polarized MDCK II cells, they were infected with viruses through the upper chamber at an m.o.i. of 0.001. After binding for 1 h, the culture medium in the upper chamber was changed to infection medium. The culture medium from upper and lower chamber was harvested separately at 8 h, 24 h, 34 h and 48 h post infection and virus titer was determined by HA-assay.

**Photocholesterol crosslinking of HA**

Two different experiments, labeling of HA-expressing cells or immunoprecipitated HA, were performed to investigate whether HA-wt and HA with mutations in the CCM interact with click-photocholesterol (6,6'-Azi-25-ethinyl -27-norcholestan-3ß-ol, see supplementary file 1 for synthesis of the compound). For the first experiment, CHO cells in 6-well plates were transfected with HA-wt, HA-LA, HA-YK2A, HA-LW2A or HA-YKLW4A cloned into the vector pCAGGS. 4-6 h post transfection, 5 µl photocholesterol (from 5 mg/ml stock in ethanol, final concentration is 50 µM) was added to 1ml of medium without serum and cells were incubated overnight. 24 hours after transfection cells were put on ice and exposed to UV light (wavelength 320–365 nm, power 8W, 3.5 A, 60V) for 10 minutes to activate the diazirine group. Cells were then lysed in 500 µl 1% NP40 in IP buffer (500 mM Tris-HCl, 20 mM EDTA, 30 mM sodium pyrophosphate decahydrate, 10 mM sodium fluoride, 1 mM sodium orthovanadate, 2 mM benzamidine, 1 mM PMSF, 1 mM NEM and protease

198 inhibitor cocktail (Sigma)). 450 µl (=90%) of the cell lysate was incubated with
199 anti-HA2 antiserum (1:1000) at 4°C with agitation overnight. 50 µl of
200 protein-A-sepharose was added to the mixture and incubated at 4°C for another 4h
201 prior to pelleting and washing with IP-buffer (2x) and with PBS.
202 For cholesterol crosslinking of purified protein, HA was first immunoprecipitated
203 from transfected CHO cells, 0.5 µl photocholesterol was added to immunoprecipitated
204 HA (in 100 µl PBS) and the mixture was illuminated with UV light at 4°C for 10
205 minutes.
206 HA-photocholesterol complexes were then clicked to Pico-azido picolyl sulfo cy3 by
207 using the CuAAC Biomolecule Reaction Buffer Kit (Jena Bioscience). Samples were
208 subjected to SDS-PAGE and HA-photocholesterol was visualized using the Typhoon
209 FLA 9500 scanner (Excitation =555 nm; Emission =565 nm) in the native (unfixed)
210 gel. In both experiments 50 µl (10%) of cell lysate was removed for western blotting
211 to compare HA-wt and HA-YKLW4A expression levels. The density of HA bands of
212 the western-blot and the fluorogram were analyzed with Image J software. The
213 photo-crosslinking (fluorogram) to protein expression (western-blot) ratios were
214 calculated for each mutant and experiment and results were normalized to HA
215 wild-type = 100%. Results are show as mean plus/minus standard deviation.
216

217 **SDS-PAGE, Western-blot and HA2 antiserum**

218 After sodium dodecyl sulfate-polyacrylamide gel electrophoresis (SDS-PAGE) using
219 12% polyacrylamide, gels were blotted onto polyvinylidene difluoride (PVDF)

membrane (GE Healthcare). After blocking of membranes (blocking solution: 5% skim milk powder in PBS with 0.1% Tween-20 (PBST)) for 1h at room temperature, anti HA2 antibodies (diluted 1:2000 in blocking solution) were applied overnight at 4°C. After washing (3x10 min with PBST), horseradish peroxidase-coupled secondary antibody (anti-rabbit, Sigma-Aldrich, Taufkirchen, Germany, 1:5000) was applied for 1 hour at room temperature. After washing, signals were detected by chemiluminescence using the ECLplus reagent (Pierce/Thermo, Bonn, Germany) and a Fusion SL camera system (Peqlab, Erlangen, Germany). The density of bands was analyzed with Image J software.

Antisera against the HA2 subunit of FPV were generated in rabbits. Purified virus was subjected to SDS-PAGE and the Coomassie-stained HA2 band was cut from the gel and used for immunization.

**Determination of the cholesterol concentration**

Cholesterol concentration in purified virus was determined using Amplex™ Red Cholesterol Assay Kit (Molecular Probes, Thermo Fisher) according to manufacturer's instruction. Briefly, virus preparations (5 µl) purified from MDCK II cells with a 20-60% sucrose gradient were lysed in 1X reaction buffer (0.1 M potassium phosphate, pH 7.4, 50 mM NaCl, 5 mM cholic acid, 0.1% Triton X-100) and incubated with working solution (300 µM Amplex Red reagent, 2 U/mL Horseradish peroxidase, 2 U/ml cholesterol oxidase in 1X reaction buffer) at 37°C for 30 min in the dark. Cholesterol oxidase produces $H_2O_2$ that in the presence of

242 horseradish peroxidase (HRP) reacts with the Amplex Red reagent in a 1:1
243 stoichiometry to produce highly fluorescent resorufin. Its fluorescence was measured
244 using a microplate reader with an excitation wavelength of 555 nm and emission at
245 590 nm. We measured only cholesterol, not cholesterol esters, since virus samples
246 were not treated with cholesterol esterase.
247 The protein concentration of the same virus preparations was measured with
248 Roti-Quant universal kit (Carl Roth), which is based on the bicinchoninic acid (BCA)
249 assay, except that PCA, a highly similar, but brighter molecule was used.
250
251 **Confocal microscopy**
252 To study apical transport of HA with single or double mutations in the CCM (LA,
253 YK2A and LW2A), polarized cells were infected with the respective viruses at an
254 m.o.i of 1. Cells were fixed with 4% formaldehyde in PBS at 6 h post infection for 20
255 min and blocked with 3% BSA in PBS. Anti-HA2 antiserum (1:500) and monoclonal
256 antibody against the basolateral marker ß-catenin (1:500) was then incubated with
257 cells, followed by anti-rabbit secondary antibody coupled to Alexa Fluor 568 (red)
258 and anti-mouse Alexa Fluor 488 (green) , respectively, both at a dilution of 1:1000.
259 To study the apical transport of the HA mutant YKLW4A, $5x10^5$ MDCK II cells were
260 seeded into 24 mm transwells one day before transfection using Lipofectamine 3000
261 Reagent (Invitrogen). 6 h post transfection, the upper chamber was changed to fresh
262 DMEM supplemented with 2% FCS. The cells were cultured for 4 more days with
263 changing medium every day. Cells were fixed with 4% formaldehyde in PBS for 20

min and permeabilized with 0.5% Triton X-100 for 5 min, followed by staining with primary antibody and secondary antibody as described above.

Cells were visualized with the VisiScope confocal FRAP System (VisiTron Systems GmbH), equipped with iXon Ultra 888 EMCCD camera, using 100X objective (1.45 NA) and illuminated via laser lines at 488 nm (Alex Fluor 488) and 561 nm (Alexa Fluor 568). Polarized cells were recorded in z-stacks with 0.5 µm increments and analyzed with Image J software.

**Membrane fusion assays**

*Hemolysis assay with virus particles*

Culture supernatants of virus-infected MDCK II cells were cleared by low-speed centrifugation (2000 x g, 5 min) and were then adjusted with infection medium to a HA titer of $2^6$. 100 µl virus was added to 96-well plates with round bottom, mixed with 100 µl 2% chicken red blood cells (RBCs) in PBS and incubated at 4°C for 30 min. To pellet RBCs with bound virus samples were centrifuged at 250xg for 1 min. After removal of supernatant, the virus-RBC sediment was resuspended in 100 µl citric acid buffer (20 mM citric acid, 150 mM NaCl) adjusted with HCl to various mildly acidic pH values and incubated at 37°C for 1 h (or different time points between 0.5 and 4 h) to allow fusion between virus and RBCs. Then the plate was centrifuged at 250 g for 1 min and 50 µl of the supernatant was removed to determine the hemoglobin released from RBCs at a wavelength of 405 nm using a microplate reader.

To increase the cholesterol content in the viral membrane prior to hemolysis, 6 µl cholesterol stock (10 mM in chloroform: methanol (1:1; v:v)) was dried under nitrogen and resuspended in 150 µl methyl-ß-cyclodextrin (MßCD) solution (2 mM in aqua dest) which gives a molar ratio of 1:5 (0.4 mM/2mM). The mixture was shaken at 37°C overnight to load MßCD with cholesterol. Viruses grown in MDCK II cells were pelleted through a 20% sucrose cushion, resuspeded in 1X TNE buffer (10 mM Tris, 100 mM NaCl und 1 mM EDTA, pH 7.4) and adjusted to the same HA titer. 100 µl virus was incubated with 100 µl cholesterol-MßCD complex at room temperature for 30 min, centrifuged at 100000 g for 20 min to pellet the virus, which was then resuspended in 1xTNE buffer. 10 µl virus with an HA titer of $2^8$ loaded or not loaded with cholesterol was used for hemolysis assay.

*R18 fluorescence dequenching assay with virus particles*

Culture supernatants of virus-infected MDCK II cells were cleared by low-speed centrifugation (2000 x g, 5 min). Viruses were pelleted (100000 x g, 2 h) through a 20% sucrose cushion, resuspended in 1X TNE buffer (10 mM Tris, 100 mM NaCl, 1 mM EDTA, pH 7.4) and adjusted to a HA titer of $2^{10}$. For octadecyl rhodamine B chloride (R18) labeling, 50 µl virus was mixed with 0.5 µl 2 mM R18 (20 µM final concentration) and incubated on ice for 30 min in the dark. To remove unincorporated R18 samples were centrifuged at 100000 xg for 15 min at 4°C, labeled viruses were resuspended in 50 µl PBS and either used immediately or stored at -80°C.

To prepare erythrocyte ghosts, human RBCs were washed three times with PBS, lysed in ice-cold hypotonic buffer (4.7 mM $Na_2HPO^4$, 1.1 mM $NaH_2PO^4$, 1 mM EDTA,

pH7.4) and again washed with PBS. For the fusion assay, 10 µl R18 labeled virus was incubated with 40 µl erythrocyte ghosts (1 mg/ml) at 4°C for 20 min. The virus-ghost mixture was then added to 1.96 ml prewarmed fusion buffer (150 mM NaCl, 10 mM Na-acetate x 3 $H_2O$, pH 7.4) in a cuvette with a magnetic stir bar. Fluorescence intensity (Exitation: 560 nm, Emmission: 590 nm) was recorded at 37°C using the Cary Eclipse fluorescence spectrophotometer (Agilent Technologies). 100 s later when the fluorescence is steady, 7 µl citric acid (250 mM) was added to lower the pH to 5. 10 min after adding citric acid, 50 µl Triton X-100 (1% in aqua dest.) was added to the solution to achieve maximal dequenching. The fusion efficiency was calculated by the formula FDQ=100×(F(t)-F(0))/(F(max)-F(0)), with F(0) as the fluorescence intensity before adding citric acid, F(max) as the maximal dequenching intensity after adding Triton X-100 and F(t) as the fluorescence intensity at each time point. The equation used for curve fitting is $f(x) = a * \left[1 - e^{(-kx)}\right]$

*Double-labelled erythrocyte fusion assay with expressed HA*

Human RBCs (1% in PBS) were double labeled with the lipidic dye R18 and the content marker calcein-AM (Molecular Probes, Life technologies). 20 µl of R18 (1 mg/ml in ethanol) was added to 1% RBC and incubated for 30min at room temperature in the dark. Samples were then washed twice with PBS and resuspended in 2 ml PBS. Calcein-AM (50 µg freshly dissolved in 10 µl DMSO + 40 µl PBS) was added to the mixture and incubated for 45 min at 37°C in the dark. The labelled RBCs were then washed with PBS five times and resuspended in 5 ml DPBS+. CHO cells in 6-well plate were transfected with HA-wt or HA-YKLW4A cloned into the pCAGGS

vector. 24 h post transfection, cells were treated with 500 µl trypsin (5 µg/ml) plus neuraminidase (from *Clostridium perfringens*, 0.22 mg/ml, Sigma) in DPBS+ for 5 min at room temperature. The reaction was stopped by adding medium and cells were washed twice with DPBS+. 1 ml double-labeled RBCs were then added to HA-expressing cells and incubated at room temperature in the dark with gentle shaking. Unbound RBCs were removed by washing twice with DPBS+. DPBS+ adjusted with HCl to pH 5 was added to cells and incubated for 5min at 37°C. Acidic DPBS+ was replaced by DPBS+ adjusted to neutral pH and after incubation for 10 min cells were observed in an inverted fluorescence microscope (Zeiss, calcein channel: Excitation: band pass filter 470/540, Emission: BP 525/50; R18 channel: Excitation = BP 572/625 Emission =BP 629/662).

## RESULTS

### Mutation in the CCM decrease cross linking of HA to photocholesterol

The ectodomain of HA is connected by a nine amino acid long and flexible linker (that contains the cleavage sites for proteases used to remove the ectodomain from virus particles (39-41)) to the 26 amino acid long, α-helical transmembrane region (TMR) (42-44) and the eleven amino acid long cytoplasmic tail carrying three fatty acids attached to conserved cysteine residues (28, 45). Only HAs of the phylogenetic group 2 contain a CCM motif, comprising the conserved amino acids YK at the end of the linker and LW at the beginning of the TMR (Fig. 1A). A helical wheel plot revealed that the amino acids K, L and W are located on one, but Y on the other side of a helix suggesting that two helices of the trimeric HA molecule must contribute to binding of one cholesterol molecule (Fig. 1B). This distribution is thus similar to the amino acids that interact with cholesterol in 7TMR receptors, where the residues W/Y-I/V/L-K/R are on one helix, but another aromatic amino acid, either phenylalanine (F) or tyrosine (Y) on a second helix that bind cholesterol from the other side (32, 35, 36). The cholesterol binding site in the ß2-adrenergic receptor is located in the internal part of the transmembrane region and is completely embedded within the membrane (32), but other 7TMR receptors bind cholesterol to the outer part of the TMR or to amino acids that do not correspond to the CCM motif (35).

In our previous studies we reported that various mutations in the CCM severely retard transport of HA to the plasma membrane (31, 37), but whether the CCM interacts with cholesterol was not investigated. We performed experiments with a

363 clickable–photocholesterol that contains a diazirine group at position 6 of the sterol
364 ring (Fig. 2A). This moiety disintegrates upon uv-illumination into molecular nitrogen
365 plus a highly reactive carbene-group that forms a covalent bond with amino acid side
366 chains in close vicinity. To visualize cross-linked proteins, click-photocholesterol
367 contains a terminal alkine group at the end of the side chain which can be “clicked” in
368 a copper-catalyzed reaction under physiological conditions to the azido-fluorophore
369 Cy3. A similar, but tritiated compound was used to demonstrate cholesterol-binding to
370 synaptophysin (46) and another study showed that this photocholesterol is a faithful
371 mimetic of authentic cholesterol (47). It is also more similar to genuine cholesterol
372 than other photocholesterol probes used recently since it contains (besides the alkine
373 group) no further alterations in cholesterol´s alkyl side chain (48). However, some of
374 the diazirine groups might be photoactivated to other reactive species that have a
375 longer half time than the carbene-group. They might then be cross-linked
376 unspecifically to any proteins they encounter during diffusion through the membrane.
377 Thus, photocrosslinking is a qualitative rather than a quantitative measure of the
378 cholesterol affinity of a protein. Nevertheless, all available compounds label only a
379 few specific proteins out of all cellular membrane proteins (46, 48) indicating that
380 they are suitable tools to identify proteins that strongly (but non-covalently) interact
381 with cholesterol.
382 We expressed H7 subtype HA from a variant of fowl plague virus (FPV*) having a
383 monobasic cleavage site, both the wild-type protein and a mutant where the four
384 amino acids forming the CCM were replaced by alanine (HA YKLW4A). In the first

385 experiments transfected CHO cells were labeled with click-photocholesterol for 16
386 hours and subsequently uv-irradiated for 10 minutes. Cells were then lysed, one
387 aliquot was subjected to western-blotting with HA2 specific antibodies, the other
388 aliquot to immunoprecipitation using the same antibodies and click-chemistry. The
389 resulting fluorescence scan showed incorporation of photocholesterol into both HA wt
390 and HA YKLW4A in approximately similar amounts (Fig. 2C). However, the western
391 blot revealed that the expression level of HA YKLW4A is significantly higher (Fig.
392 2B). Quantification of fluorescence intensities and normalizing them to the expression
393 level showed that incorporation of photocholesterol into HA YKLW4A was reduced to
394 58% (±13%, mean of six transfections, Fig. 2D).
395 Since mutations in the CCM decrease association of HA with nanodomains (27, 37)
396 one might argue that the diminished labeling of HA YKLW4A might be due to its
397 compartmentalization into cholesterol-depleted membrane domains. Consequently,
398 less cholesterol (and hence photocholesterol) is present in the vicinity of HA
399 YKLW4A and thus available to label the protein by random interactions. To exclude
400 such an unspecific effect, we first immunoprecipitated HA wt and HA YKLW4A from
401 cell lysates and then performed photo-crosslinking and click-chemistry on the purified
402 HA-antibody complex (Fig. 2E+F). Nevertheless, a similar result was obtained;
403 incorporation of photocholesterol into HA YKLW4A was even more reduced relative
404 to HA wt (38 ±5%, mean of four transfections, Fig. 2G).
405 To determine whether partial exchange of the CCM has an effect on
406 photo-crosslinking we created HA double mutants HA LW2A and HA YK2A where

two consecutive amino acids located at the end of the TMR and in the linker region, respectively were exchanged by alanine. In HA LA the leucine in the TMR (which of all single mutants had the strongest effect on intracellular transport of HA (37)) was substituted by alanine. Cells expressing the three HA mutants were labeled and analyzed as before but no significant reduction of incorporation of photocholesterol was detected (Fig. 2H-J). Thus, in order to reduce photo-crosslinking of HA the whole CCM must be exchanged suggesting that the residues act synergistically with cholesterol.

**Mutations in the CCM of HA affect virus replication**

All our previous experiments about the CCM of HA were performed with expressed protein (37). To investigate whether cholesterol binding to HA affects virus replication, we created the described mutations in the CCM of HA in the context of the viral genome. We used a variant of fowl plague virus (A/FPV/Rostock/34, H7N1), termed FPV* which contains a monobasic cleavage site in HA and thus requires trypsin for growth in cell culture (38). The amino acid exchanges were generated by at least three nucleotide substitutions to exclude that mutant viruses revert back to wild type.

The mutant HA plasmid together with plasmids encoding the other viral proteins were transfected into HEK 293T cells, the supernatant was used to infect MDCK II cells and release of virus particles was assessed by HA assays. In three independent transfections we never rescued virus particles for FPV* YKLW4A, whereas wild-type virus and the other three mutants done in parallel exhibit HA titers of $2^5$-$2^6$. From the

rescued mutants a virus stock was generated in MDCK II cells and sequencing of the HA gene showed that the desired mutations were still present (data not shown).

To compare the replication kinetics of the viruses, MDCK II cells were infected with FPV* wt or with the mutants at an m.o.i. of 0.0005 (based on TCID50 titer), supernatants were collected at various time points post infection and virus titers were assessed by HA and TCID 50-assay (Fig. 3A+B). The growth curve revealed a statistically significant decrease in the TCID 50 titer for FPV* LW2A (1.5 logs, ~95% reduction, mean of 3 experiments) at 36 and 48 hours post infection. Titers of FPV* YK2A and FPV* LA were also somewhat decreased relative to FPV* wt.

We next asked whether mutating the CCM of HA might reduce the competitive fitness of the virus. To test this, we mixed FPV* YK2A or FPV* LW2A with FPV* wt at a ratio of 5:1, co-infected MDCK II cells (total moi of 0.0005), extracted viral RNA from cellular supernatants, either before or at 24 and 48 hours after infection, amplified the relevant part of the HA gene with rtPCR and analyzed it by sequencing. Fig. 3C shows the sequencing chromatograms for the region of interest in the HA gene. Both wild-type and mutant viruses were detected at all time points, reflected by superimposed peaks for the respective nucleotide bases at the mutation site. Due to the higher number of infectious mutant viruses in the inoculum the mutant sequence is predominant before infection, but particles released from cells after 24 and 48 hours contain mainly the wild type sequence. Although the differences in the peak heights in the chromatograms should not be interpreted in a precise quantitative manner, it is obvious that the wild type virus rapidly outgrows mutant virus with two exchanges in

451 the CCM within a few replication cycles.

452 In sum, we conclude that the CCM is essential for virus replication. Exchanging all
453 four amino acids of the motif prevented generation of infectious virions and
454 exchanging two of them reduced virus titers and their competitive fitness.

455

456 **Mutations in the CCM do not cause mistargeting of HA in polarized cells**

457 In polarized MDCK cells HA is transported to the apical membrane, the viral budding
458 site (49). Since signals for transport are located in the TMR of HA (50-52) we
459 analyzed whether mutations in the CCM disturbed polarized budding of virus particles.
460 MDCK cells grown on transwell filters were infected with FPV* wt and FPV* mutant
461 virus at low moi, aliquots of the supernatant were removed from the apical and
462 basolateral chamber at various time points and virus titers were determined using
463 HA-assays. The growth curve plotted for virus particles released from the apical
464 membrane shows again a reduction in virus titers for all FPV* mutants, statistically
465 significant for FPV* LW2A. However, no virus was released for any of the mutants
466 from the basolateral membrane (Fig. 4A). Since Influenza virus might bud from the
467 apical membrane even if HA is redirected to the basolateral membrane (53) we also
468 determined the localization of HA LA, HA LW2A and HA YK2A in virus-infected
469 and of HA YKLW4A in transfected cells using confocal microscopy. However, wt HA
470 and all mutants are exclusively located at the apical membrane, the fluorescence
471 derived from anti-HA antibodies does not overlap with the fluorescence emitted by
472 the basolateral membrane marker (Fig. 4B+C). We conclude that mutations in the

473 CCM do not affect targeting of HA to the apical membrane.

474

475 **Mutations in the CCM reduce incorporation of HA and cholesterol into virions**

476 In principle, the decrease in virus replication could be due to compromised cell entry
477 of mutant virus and/or a defect in virus assembly and budding. We have previously
478 shown that mutations in the CCM decreases HA´s cell surface exposure and
479 association with membrane rafts in transfected cells (37). Since these defects might
480 affect incorporation of HA into budding virions we purified FPV* wt and FPV*
481 LW2A virus particles with sucrose gradient centrifugation from embryonated eggs
482 and analyzed their protein composition by SDS-PAGE and Coomassie staining (Fig.
483 5A). Densitometry of viral protein bands and calculation of the viral protein ratios
484 (Fig. 5B) revealed for FPV* LW2A reduced amounts of HA relative to NP (85%,
485 normalized to FPV* wt) and to M1 (82%). If virus particles were purified from
486 MDCK II cells (Fig. 5C), the reduction in HA incorporation was even more
487 pronounced; the HA/M1 ratio is reduced to 59% and the HA/NP ratio to 68%.
488 Likewise, the other two mutants also exhibit a (albeit less distinct, 82-90%) reduction
489 in the HA content (Fig. 5D).
490 Since mutations in the CCM reduce association of HA with membrane nanodomains
491 (27, 37) and since FPV wt buds through cholesterol-enriched domains (5) we asked
492 whether FPV* mutants possess less cholesterol in their membrane. We therefore
493 determined the cholesterol concentration of the same three virus preparations from
494 MDCK II cells and divided it by the protein concentration. For FPV* wt we

495 determined a mean of 220 nM cholesterol per ng/µl total protein, but considerable
496 variations between individual preparations was observed. Nevertheless, the
497 cholesterol content of each FPV* mutant was lower in every (except one) virus
498 preparation relative to FPV* wt, which was purified from sister cultures in parallel.
499 The only exception was FPV* LA for which a slightly higher amount of cholesterol
500 was determined in one, but not in the other two preparations (see Fig. 6A for details
501 on individual experiments).

502 Normalizing the cholesterol content for each virus preparation (wt =100%) exhibit a
503 reduction to 89% in FPV* LA, to 88% in FPV LW2A and to 82% in FPV YK2A (Fig.
504 6B). Assuming that our FPV* wt preparations contain 52 mol% of cholesterol in
505 relation to all other envelope lipids as determined by quantitative mass spectrometry
506 for FPV particles grown in the same cell type (5), one can calculate that the
507 cholesterol content in mutant particles is reduced to 46% in FPV* LA and FPV*
508 LW2A and to 43% in FPV* YK2A. This corresponds quite exactly to the cholesterol
509 content (45%) determined for the apical membrane of polarized MDCK II cells (5).
510 Thus, our results are consistent with the concept that viruses with mutations in the
511 CCM bud not through (cholesterol-enriched) membrane nanodomains but through the
512 bulk phase of the plasma membrane (26).

513 Influenza A virus mutants with defects in virus assembly and budding release particles
514 with aberrant morphology (54). We therefore investigated the virus preparations also
515 by negative stain electron microscopy, but no differences in the morphology or size of
516 intact virus particles were obvious (data not shown). Whether, the lower cholesterol

517 content affects the density of HA spikes in virus particles requires investigations with
518 more sophisticated methods (25).
519
520 **Mutations in the CCM decrease the hemolytic activity of HA**
521 Next, we investigated whether mutations in the CCM affect cell entry of viruses via
522 HA-mediated membrane fusion. Since the extent of membrane fusion increases with
523 the HA-concentration and since the HA amount is reduced in mutant virus
524 preparations (Fig. 5A-D) we first used hemolysis assays. This allows adjusting the
525 amount of virus by means of its HA-titer and to record membrane fusion
526 quantitatively by measuring the release of hemoglobin.
527 In the first set of experiments we compared the pH dependence of hemolysis. Wild
528 type and mutant virus with an HA-titer of $2^6$ were adsorbed to chicken erythrocytes,
529 the pH was adjusted to mildly acidic pH values between 5 and 7, erythrocytes with
530 bound virus were incubated for 60 min at 37°C and hemoglobin release was
531 determined spectroscopically. Beginning with pH 5.7 FPV* wt causes hemoglobin
532 release; the amount increased linearly with decreasing pH values (Fig. 7A) which is in
533 agreement with published data on the fusion activity of the closely related H7
534 Weybridge strain (55). All mutant viruses also start to cause hemolysis at pH 5.7, but
535 the amount of released hemoglobin is reduced to ~ 30% with each virus and at all pH
536 values. We also compared the kinetics of hemolysis by incubating pH 5 activated
537 viruses for up to four hours with erythrocytes. The amount of released hemoglobin
538 increases linearly with time for all viruses, but the slope of the line is much steeper

539 with FPV* wt. At every time point the amount of released hemoglobin is clearly lower
540 when using mutant virus particles (Fig. 7B).
541 Withdrawal of cholesterol from the viral membrane negatively and addition of
542 cholesterol positively affect HA´s membrane fusion activity (22, 23, 56, 57). In
543 principle, the defect in the fusion activity of mutant viruses might be either due to
544 altered biophysical properties of the viral membrane caused by their reduced
545 cholesterol content or due to a more local or intrinsic functional defect in the HA
546 molecule. To distinguish between both possibilities, we replenished the viral
547 membrane with cholesterol by incubation of virus particles with cyclodextrin fully
548 loaded with this lipid. Cholesterol measurements of virus preparations before and
549 after incubation with cyclodextrin revealed for FPV* wt and all mutant viruses a
550 cholesterol increase of ~20-35%; mutant viruses have now a cholesterol content
551 similar to or slightly higher than FPV* wt before cholesterol addition. Hemolysis
552 assays at pH5 showed an increase in hemoglobin release for both wild-type and
553 mutant viruses by 10% to 35% after cholesterol loading (Fig. 7D) confirming the
554 beneficial effect of cholesterol on membrane fusion. However, the hemolysis activity
555 of cholesterol-enriched mutant viruses was in each experiment lower compared to
556 untreated wild-type virus particles (Fig. 7C) indicating that the defect in membrane
557 fusion persists even if the mutant particles have a cholesterol content like wild-type
558 viruses.
559
560 **Mutations in the CCM decrease the hemifusion activity of HA**

A defect in hemolysis does not reveal which step in membrane fusion is affected, since release of hemoglobin requires lipid mixing as well as opening and widening of a fusion pore. In some HA mutants both events are uncoupled, for example HA with a glycolipid-anchor instead of the transmembrane domain (GPI-HA), causes hemifusion, but not full fusion (17). We were therefore interested whether or not viruses with mutations in the CCM of HA exhibit a defect in hemifusion. We employed the R18 dequenching assay that allows monitoring lipid mixing between erythrocyte ghosts and virus particles. The lipophilic fluorophore octadecylrhodamine (R18) is integrated into the viral envelope at self-quenching concentrations. Upon binding of washed virus particles (adjusted to an HA-titer of $2^{10}$) to ghosts and activation of HA´s fusion activity by low pH treatment, viral and ghost lipids begin to mix. This causes dequenching of R18 and the resulting fluorescence increase is recorded in a fluorescence spectrometer. Once viral membrane fusion is completed, detergent is added that causes complete lysis of membranes. The maximal dequenching of R18´s fluorescence is used to calculate the fusion activity at each time point.

Fig. 8A shows the mean relative fluorescence intensity of four fusion reactions plotted against the time course. After acidification to pH5 all FPV* viruses exhibit a rapid increase in the fluorescence intensity, which reaches a plateau after ~ 2min. FPV* wt exhibits a maximal fusion activity of 20%, which is clearly decreased in the mutants. Normalizing the extent of fusion (FPV* wt = 100%) shows a reduction to 75% for FPV* LA and to ~ 50% for the double mutants FPV* LW2A and YK2A (Fig. 8B). Furthermore, fitting the curves revealed also differences in the fusion kinetics. 36 secs

583 is the half time for maximal fusion calculated for FPV* wt and FPV* LA, but this is
584 extended to 57 secs for FPV* LW2A and FPV* YK2A. Since a similar result was
585 obtained if the R18 assay was performed at pH 5.5 (except that the half times were
586 longer for all viruses, data not shown), we conclude that mutations in the CCM of HA
587 affect both the kinetics and the extent of lipid mixing.
588
589 **HA with a complete exchange of the CCM has a defect in hemifusion**
590 Finally, we asked whether the HA mutant with a complete exchange of the CCM also
591 exhibits a defect in membrane fusion. Since no virus particles could be rescued for
592 that mutant we had to rely on a cell-based fusion assay. As target we used
593 double-labeled erythrocytes that contain R18 in their membrane and the soluble
594 fluorophore calcein in their interior. After proteolytic cleavage and acid treatment of
595 HA, R18 diffuses into the cellular plasma membrane whereas calcein stains the
596 cytoplasm which can both be monitored in the fluorescence microscope.
597 Cells expressing HA YKLW4A clearly show hemifusion (cells in the upper left
598 quadrant of Fig. 9A) and also full fusion (some cells in the right half of the figure)
599 with erythrocytes. However, the number of fusion events is clearly reduced compared
600 to HA wt, see Fig. 9B for an image of cells expressing HA YKLW4A or HA wt at
601 lower magnification. One factor contributing to the lower fusion efficiency might be
602 the retarded intracellular transport and reduced surface expression of HA YKLW4A
603 (37). However, the number of bound erythrocytes per transfected cell culture plate is
604 not obviously reduced with cells that express HA YKLW4A (micrograph in Fig. 9B)

and cells transfected with HA YKLW4A show similar hemadsorption activity as cells transfected with HA wt (not shown).

Furthermore, cells expressing HA YKLW4A show one peculiarity not observed for HA wt, namely erythrocytes tightly bound to cells after acid treatment that did not pass through either hemifusion or pore formation, i.e. no diffusion of R18 into the plasma membrane (see Fig. 9C for three examples) and of calcein into the cell´s cytoplasm (not shown) did occur. We then selected cells with at least two bound erythrocytes and determined in the fluorescence channel whether the erythrocytes are unfused, hemifused or fully fused to the cells. We then calculated the percentage of individual fusion steps for HA wt or HA YKLW4A; the total number of selected cells was normalized to 100%. Cells transfected with HA wt did not show “binding” of erythrocytes after acidification, 58% of bound erythrocytes only passed the hemifusion step and 42% exhibit full fusion (Fig. 9D). Cells transfected with HA YKLW4A revealed a similar percentage of fully fused erythrocytes (45%), but reduced percentage of hemifused (28%) and 22% of bound, but unfused erythrocytes. Thus, we conclude that HA YKLW4A exhibits mainly a defect in hemifusion and probably also in another step that precedes lipid mixing.

## DISCUSSION

### Cholesterol binding to HA

In this study we show for the first time that HA interacts with cholesterol. We demonstrate that complete exchange of the cholesterol consensus motif YK…LW in a group 2 HA (H7 subtype) by alanine greatly reduces (>50%) photo-crosslinking of a cholesterol analog to HA (Fig. 2). This was demonstrated by labeling transfected cells with photocholesterol and thus for HA embedded in its natural lipid environment where photocholesterol must compete with other membrane lipids for the binding site in HA. Furthermore, a similar result was obtained for purified HA immunoprecipitated from cell lysates excluding the possibility that the stronger labeling of HA wt is due to its integration into cholesterol-enriched nanodomains. HA with an exchange of two consecutive amino acids YK and LW by alanine did not reveal reduced labeling with photocholesterol (Fig. 2) suggesting that the residues synergistically interact with cholesterol. However, note that photocrosslinking is a qualitative tool to measure the cholesterol affinity of a protein and may not represent equilibrium concentrations of protein-cholesterol complexes. To more precisely determine the amino acids in HA which contact cholesterol more sophisticated methods, such as NMR or crystallography are required (36).

Our data are at odds with a recent report showing by high-resolution secondary ion mass spectrometry that HA clusters at the plasma membrane of transfected cells were not enriched with cholesterol (59). However, the observation was made with an H2 subtype HA belonging to the phylogenetic group 1 that does not contain the YKLW

644 motif. Although HA clusters at the plasma membrane have been observed both for
645 group 1 (e.g. H2, (6)) and group 2 HAs (e.g. H3, H7, (7, 9, 27)) their mechanism of
646 clustering might be different. Interestingly, protease digestion experiments and
647 molecular dynamics simulations revealed that the TMR of group 2 HAs have a more
648 compact and protease-resistant quaternary structure compared to the TMR of group 1
649 HAs (39).

650 The CCM is not only present in the consensus sequence of HAs of subtypes H3, H4,
651 H7, H10, H14 and H15 (Fig. 1B), the amino acids YK...LW are also completely (99%)
652 conserved within each subtype (60, supplementary file 1) arguing in favor for an
653 essential role. Indeed, infectious virus particles could not be rescued if the CCM is
654 completely exchanged; viral titers are lower if two amino acids are replaced. The
655 mutant viruses are rapidly outgrown by wild-type indicating that they have a
656 comparative fitness disadvantage (Fig. 3). It is thus safe to conclude that the CCM
657 (and thus its interaction with cholesterol) is essential for Influenza virus replication,
658 affecting both virus assembly and its cell entry via membrane fusion as discussed
659 next.

660 Group 1 HAs do not possess the YK…LW motif, but contain the fairly conserved
661 motif Y-K/Q…I-Y which also corresponds to the CCM defined for 7TMR
662 (F/Y-R/K-I/V/L-Y/W). In addition, various rather loosely defined cholesterol
663 recognition motifs exist that share a similar pattern of basic, aromatic and large
664 hydrophobic amino acid (34). However, mutations at the boundary between the linker
665 region and external part of the TMR do not retard transport of group 1 HAs to the

plasma membrane (51). Note also that a tyrosine which is important for the recently determined structure of the TMR region of a group 1 HA (residue 18 in Fig 1a, (42)) is not conserved in group 2 HAs suggesting that both phylogenetic HA groups might exhibit different structures in this region.

**The role of the CCM for apical transport of HA and for virus assembly and budding**

Mutations in the CCM did not have an effect on apical budding of virus particles from polarized cells and did not affect transport of HA to the apical membrane (Fig. 4). Although signals for apical transport of HA are located in the TMR they do not overlap with signals that mediate inclusion of HA into detergent-resistant membranes a surrogate marker for association with cholesterol enriched nanodomains (52).

However, the cholesterol content of mutant virus particles is significantly decreased by 10% (mutant LW2A) to 20% (YK2A, see Fig. 6). Assuming that the membrane of one spherical Influenza virus particle contains a total of 300.000 lipid molecules (as calculated for HIV particles that have the same size and hence lipid surface area (61) and ~ 50% (=150.000) are cholesterol (5), a decrease of 10-20% is equivalent to 15.000-30.000 cholesterol molecules. An average Influenza virus particle contains 300-500 trimeric HA spikes (as determined by Cryo-EM, (62, 63)) and thus at most ~ 1500 cholesterol binding sites are available. Based on this estimation it is evident that the 10-20% reduction in the cholesterol content cannot be explained by a stoichiometric (1:1) binding of cholesterol to HA. Instead, a cooperative effect must

688 be involved; the mutation in the CCM decreases the cholesterol content by 10-20
689 cholesterol molecules per trimeric HA spike. One cholesterol molecule in direct
690 contact with HA´s CCM recruits (possibly by lipid-lipid interactions) other steroid
691 molecules into virus particles. This assumption is supported by crystal structures of
692 the β-adrenergic and other 7TM-receptors that exhibit two (or more) parallel aligned
693 cholesterol molecules, but only one interacts directly with the CCM motif (35).
694 10-20 cholesterol molecules would be sufficient to encase the outer part of
695 transmembrane domain of one trimeric HA spike if we assume an α-helix and
696 cholesterol diameter of 1 and 0.5 nm, respectively. Such a lipid shell has been
697 postulated to target transmembrane proteins to lipid domains or induce the formation
698 of domains in a membrane that is poised to do so but is not yet phase-separated (64,
699 65). Accordingly, the HA mutants YK2A and LW2A revealed reduced fluorescence
700 resonance energy transfer (FRET) with a double-acylated raft-marker in transfected
701 cells (37) and exchange of three amino acids at the beginning of the transmembrane
702 region prevents raft-dependent clustering of H3-subtype HA at the plasma membrane
703 (26). Mistargeting of HA might cause budding of virus particles through the
704 (cholesterol-depleted) bulk phase of the plasma membrane. In accordance, the
705 reduction of 10-20% cholesterol molecules in mutant virus particles is equivalent to a
706 total cholesterol content of 45%, which corresponds to the cholesterol content
707 determined for the whole apical membrane of polarized MDCK II cells (5).
708 Mutations in the CCM do not only affect the lipids in the viral membrane, but also
709 reduce incorporation of HA (relative to M1 and NP) into particles. This was evident

not only with viruses grown in MDCK II cells, but also (but less distinct) in embryonated eggs. The effect was most pronounced if the two amino acids LW in the TMR were exchanged (Fig. 5). A similar observation was made for H3 subtype HA from the filamentous Udorn strain having an exchange of the amino acids WIL at the beginning of the TMR (26). A priori one would rather assume that the HA content of mutant virus particles increases if viruses bud through the bulk phase of the plasma membrane but all other viral proteins are still mainly targeted to the original virus assembly site. However, assembly of viral proteins at the plasma membrane is a complicated process dependent on intrinsic signals in viral proteins as well as (partly transient) protein-protein interactions (8, 11, 12).

The mutation LW2A had the strongest effect on replication of virus in cell culture (Fig. 3B, 4A) and on HA incorporation into virus particles (Fig. 5), whereas the cholesterol content was reduced in the mutant YK2A to a larger extent compared to LW2A (Fig. 6). Note, however, that the data on the composition of virus particles show considerable variation between experiments, which is at least partly due to the pleomorphic nature of Influenza viruses. A recent study showed that even genetically homogenous virus particles released from a single infected cell show enormous variation in size and protein composition, i. e. the copy number of individual proteins vary up to 100 fold between virions (66). This low-fidelity assembly process makes it complicated to more precisely determine the effect of mutations on the morphology of Influenza virus particles.

An open question is the functional relationship between the two intrinsic nanodomain

732 targeting signals in HA, S-acylation at cytoplasmic cysteine residues and the
733 cholesterol-binding amino acids at the beginning of the TMR. Removal of only one
734 signal is sufficient to perturb raft association of HA (27, 29, 30). Both signals are
735 essential for virus replication; their complete removal prevented creation of
736 recombinant virus particles (this study and (18, 60, 67)). Viruses with partially deleted
737 signals could be generated but revealed lower titers and defects in virus budding and
738 membrane fusion (18, 26, 67). Otherwise, effects of mutating the two
739 nanodomain-targeting signals are different. Removal of the acylation sites does not
740 retard intracellular transport of HA (31, 68) and does not change the lipid composition
741 (cholesterol content) of the viral membrane, at least not if virus-like particles were
742 analyzed (69). How the functions of both raft-targeting signals interact to define the
743 viral budding site remains unclear.
744 However, the interaction of HA with cholesterol does not necessarily occur only at the
745 plasma membrane since the HA mutants exhibit strongly retarded transport through
746 the Golgi (37), the part of the exocytic pathway in which the cholesterol concentration
747 successively increases from ~5% (ER) to ~40% (plasma membrane) (58).
748

749 **The role of the CCM for membrane fusion**

750 With three different assays using either virus particles or HA-expressing cells we
751 show that mutations in the CCM of HA decrease both the kinetics and the extent of
752 HA´s fusion activity. A similar result was reported for H3-subtype HA that contains
753 mutations at three amino acids at the beginning of the transmembrane region (26).

One contributing factor might be the reduced amount of HA at the surface of transfected cells (37) and in virus preparations (Fig. 4). However, we (at least partly) corrected for the latter by adjusting wild type and mutant viruses to the same HA-titer prior to the fusion assay. Thus, it is likely that the fusion defect is not (only) due to lower numbers of HA molecules at the fusion site, but a direct consequence of the mutations in the CCM of HA.

The R18 lipid mixing assay with mutant virus particles YK2A and LW2A as well as quantification of individual fusion events of HA YKLW4A-expressing cells revealed that the mutations in the CCM mainly affect the stage of lipid mixing (Fig. 7-9). Cells expressing HA YKLW4A showed another peculiarity, namely unfused erythrocytes still bound to their surface after low pH treatment (Fig. 9). In principle, this could be a fraction of HA YKLW4A molecules not activated by the low pH treatment and hence still bound in its pH 7 conformation to sialic-acid containing receptors on red blood cells. Alternatively, this HA YKLW4A fraction might have executed the first conformational change but has not completed the refolding step that causes fusion between viral and cellular membranes (1). In that case the fusion peptide has been exposed and inserted into the membrane thereby stabilizing the interaction between HA-expressing cells and erythrocytes at acidic pH. Our observation of tightly bound, but unfused erythrocytes to HA-expressing cells might correspond to early stages of HA-mediated membrane fusion recently observed by Cryo EM, e.g. HA-bridging, membrane dimpling and/or tightly docked membrane interfaces (70, 71). In any case, it suggests, that HA YKLW4A also has a defect in a membrane fusion step prior to

776 lipid mixing.

777 The reduced fusion activity of HA might be due to a global effect of the mutations in
778 the CCM on the viral membrane. Virus particles exhibit reduced cholesterol content,
779 and this might profoundly affect biophysical properties of the membrane beneficial
780 for fusion (22, 23, 25, 56)). Indeed, when we loaded mutant virus particles with
781 additional cholesterol the hemolysis activity increased (Fig. 7D). Nevertheless,
782 cholesterol-loaded mutant virus particles revealed hemolysis values well below those
783 determined for FPV* wt without additional cholesterol loading although their
784 cholesterol content is now roughly the same (Fig. 7C). Note also that the HA mutant
785 YK2A has the lowest cholesterol content in the viral membrane (Fig. 6B), but HA
786 LW2A exhibits the largest effect on virus infectivity and its hemolytic activity (Fig.
787 3+7). Thus, the fusion defect is most likely not due to a general disadvantageous
788 property of the viral membrane, such as disturbed liquid phase separation
789 (raft-formation) and/or membrane ordering. We therefore rather prefer a model
790 where a local interaction between cholesterol and the TMR of HA affects membrane
791 fusion as proposed recently (57). One might envision that the CCM recruits
792 cholesterol from the inner to the outer leaflet of the viral membrane, especially prior
793 to hemifusion. The shape of cholesterol (small headgroup, large hydrophobic tail) is
794 beneficial for the formation of a highly bended membrane intermediate, but only if
795 cholesterol is located in the external leaflet, and not in the internal leaflet of the viral
796 membrane (21, 72). Alternatively, cholesterol binding to the CCM (or more generally
797 the amino acid exchanges we introduced) might affect the flexibility of HA´s linker

798 region which may be important to facilitate the pH-dependent changes in HA
799 conformation required for membrane fusion as recently suggested (42).
800 In sum, mutations in the cholesterol consensus motif of a group 2 HA affect various
801 functionalities of the protein; its transport along the exocytic pathway, raft association
802 at the plasma membrane (37), incorporation of cholesterol and HA into budding virus
803 particles and virus entry via membrane fusion, especially lipid mixing and probably a
804 preceding step. High resolution Cryo-EM of full length of a group 2 HA embedded in
805 a membrane (similar to the one published for a group 1 HA (42)) might be helpful to
806 determine the structure of the cholesterol binding pocket as one prerequisite to
807 develop a small molecule that inactivates the virus.
808

809 **ACKNOWLEDGEMENTS**

810 This work was supported by the German Research Foundation (SFB 740 TP C3) and
811 by the Human Frontiers Science Program. Bodan Hu is recipient of a PhD fellowship
812 from the China Scholarship Council (CSC). The funders had no role in study design,
813 data collection and interpretation, or the decision to submit the work for publication.
814 We thank Ralf Wagner and Hans-Dieter Klenk (Virology, Marburg) for providing the
815 reverse genetics system used and Kai Ludwig (BioSupraMol, Chemistry and
816 Biochemistry, FU Berlin) for performing electron microcopy.

817 **REFERENCES**

818 1. Skehel JJ, Wiley DC. 2000. Receptor binding and membrane fusion in virus
819 entry: the influenza hemagglutinin. Annu Rev Biochem 69:531-69.
820 2. Whittaker GR. 2001. Intracellular trafficking of influenza virus: clinical
821 implications for molecular medicine. Expert Rev Mol Med 2001:1-13.
822 3. Scheiffele P, Rietveld A, Wilk T, Simons K. 1999. Influenza viruses select
823 ordered lipid domains during budding from the plasma membrane. J Biol
824 Chem 274:2038-44.
825 4. Simons K, Gerl MJ. 2010. Revitalizing membrane rafts: new tools and insights.
826 Nat Rev Mol Cell Biol 11:688-99.
827 5. Gerl MJ, Sampaio JL, Urban S, Kalvodova L, Verbavatz JM, Binnington B,
828 Lindemann D, Lingwood CA, Shevchenko A, Schroeder C, Simons K. 2012.
829 Quantitative analysis of the lipidomes of the influenza virus envelope and
830 MDCK cell apical membrane. J Cell Biol 196:213-21.
831 6. Hess ST, Kumar M, Verma A, Farrington J, Kenworthy A, Zimmerberg J. 2005.
832 Quantitative electron microscopy and fluorescence spectroscopy of the
833 membrane distribution of influenza hemagglutinin. J Cell Biol 169:965-76.
834 7. Leser GP, Lamb RA. 2005. Influenza virus assembly and budding in
835 raft-derived microdomains: a quantitative analysis of the surface distribution
836 of HA, NA and M2 proteins. Virology 342:215-27.
837 8. Leser GP, Lamb RA. 2017. Lateral Organization of Influenza Virus Proteins in
838 the Budozone Region of the Plasma Membrane. J Virol 91.

9. Hess ST, Gould TJ, Gudheti MV, Maas SA, Mills KD, Zimmerberg J. 2007. Dynamic clustered distribution of hemagglutinin resolved at 40 nm in living cell membranes discriminates between raft theories. Proc Natl Acad Sci U S A 104:17370-5.

10. Veit M, Thaa B. 2011. Association of influenza virus proteins with membrane rafts. Adv Virol 2011:370606.

11. Chlanda P, Zimmerberg J. 2016. Protein-lipid interactions critical to replication of the influenza A virus. FEBS Lett 590:1940-54.

12. Rossman JS, Lamb RA. 2011. Influenza virus assembly and budding. Virology 411:229-36.

13. Bottcher-Friebertshauser E, Klenk HD, Garten W. 2013. Activation of influenza viruses by proteases from host cells and bacteria in the human airway epithelium. Pathog Dis 69:87-100.

14. Chernomordik LV, Kozlov MM. 2005. Membrane hemifusion: crossing a chasm in two leaps. Cell 123:375-82.

15. Ivanovic T, Choi JL, Whelan SP, van Oijen AM, Harrison SC. 2013. Influenza-virus membrane fusion by cooperative fold-back of stochastically induced hemagglutinin intermediates. Elife 2:e00333.

16. Armstrong RT, Kushnir AS, White JM. 2000. The transmembrane domain of influenza hemagglutinin exhibits a stringent length requirement to support the hemifusion to fusion transition. J Cell Biol 151:425-37.

17. Kemble GW, Danieli T, White JM. 1994. Lipid-anchored influenza

861 hemagglutinin promotes hemifusion, not complete fusion. Cell 76:383-91.

862 18. Wagner R, Herwig A, Azzouz N, Klenk HD. 2005. Acylation-mediated
863 membrane anchoring of avian influenza virus hemagglutinin is essential for
864 fusion pore formation and virus infectivity. J Virol 79:6449-58.

865 19. Kozerski C, Ponimaskin E, Schroth-Diez B, Schmidt MF, Herrmann A. 2000.
866 Modification of the cytoplasmic domain of influenza virus hemagglutinin
867 affects enlargement of the fusion pore. J Virol 74:7529-37.

868 20. Melikyan GB, Markosyan RM, Roth MG, Cohen FS. 2000. A point mutation
869 in the transmembrane domain of the hemagglutinin of influenza virus
870 stabilizes a hemifusion intermediate that can transit to fusion. Mol Biol Cell
871 11:3765-75.

872 21. Chernomordik LV, Kozlov MM. 2003. Protein-lipid interplay in fusion and
873 fission of biological membranes. Annu Rev Biochem 72:175-207.

874 22. Biswas S, Yin SR, Blank PS, Zimmerberg J. 2008. Cholesterol promotes
875 hemifusion and pore widening in membrane fusion induced by influenza
876 hemagglutinin. J Gen Physiol 131:503-13.

877 23. Sun X, Whittaker GR. 2003. Role for influenza virus envelope cholesterol in
878 virus entry and infection. J Virol 77:12543-51.

879 24. Chlanda P, Mekhedov E, Waters H, Schwartz CL, Fischer ER, Ryham RJ,
880 Cohen FS, Blank PS, Zimmerberg J. 2016. The hemifusion structure induced
881 by influenza virus haemagglutinin is determined by physical properties of the
882 target membranes. Nat Microbiol 1:16050.

883 25. Domanska MK, Dunning RA, Dryden KA, Zawada KE, Yeager M, Kasson
884 PM. 2015. Hemagglutinin Spatial Distribution Shifts in Response to
885 Cholesterol in the Influenza Viral Envelope. Biophys J 109:1917-24.
886 26. Takeda M, Leser GP, Russell CJ, Lamb RA. 2003. Influenza virus
887 hemagglutinin concentrates in lipid raft microdomains for efficient viral fusion.
888 Proc Natl Acad Sci U S A 100:14610-7.
889 27. Engel S, Scolari S, Thaa B, Krebs N, Korte T, Herrmann A, Veit M. 2010.
890 FLIM-FRET and FRAP reveal association of influenza virus haemagglutinin
891 with membrane rafts. Biochem J 425:567-73.
892 28. Kordyukova LV, Serebryakova MV, Baratova LA, Veit M. 2008. S acylation of
893 the hemagglutinin of influenza viruses: mass spectrometry reveals site-specific
894 attachment of stearic acid to a transmembrane cysteine. J Virol 82:9288-92.
895 29. Scolari S, Engel S, Krebs N, Plazzo AP, De Almeida RF, Prieto M, Veit M,
896 Herrmann A. 2009. Lateral distribution of the transmembrane domain of
897 influenza virus hemagglutinin revealed by time-resolved fluorescence imaging.
898 J Biol Chem 284:15708-16.
899 30. Scheiffele P, Roth MG, Simons K. 1997. Interaction of influenza virus
900 haemagglutinin with sphingolipid-cholesterol membrane domains via its
901 transmembrane domain. Embo J 16:5501-8.
902 31. Engel S, de Vries M, Herrmann A, Veit M. 2012. Mutation of a raft-targeting
903 signal in the transmembrane region retards transport of influenza virus
904 hemagglutinin through the Golgi. FEBS Lett 586:277-82.

905 32. Hanson MA, Cherezov V, Griffith MT, Roth CB, Jaakola VP, Chien EY,
906 Velasquez J, Kuhn P, Stevens RC. 2008. A specific cholesterol binding site is
907 established by the 2.8 A structure of the human beta2-adrenergic receptor.
908 Structure 16:897-905.
909 33. Epand RM, Thomas A, Brasseur R, Epand RF. 2010. Cholesterol interaction
910 with proteins that partition into membrane domains: an overview. Subcell
911 Biochem 51:253-78.
912 34. Fantini J, Barrantes FJ. 2013. How cholesterol interacts with membrane
913 proteins: an exploration of cholesterol-binding sites including CRAC, CARC,
914 and tilted domains. Front Physiol 4:31.
915 35. Gimpl G. 2016. Interaction of G protein coupled receptors and cholesterol.
916 Chem Phys Lipids 199:61-73.
917 36. Yang ST, Kreutzberger AJB, Lee J, Kiessling V, Tamm LK. 2016. The role of
918 cholesterol in membrane fusion. Chem Phys Lipids 199:136-143.
919 37. de Vries M, Herrmann A, Veit M. 2015. A cholesterol consensus motif is
920 required for efficient intracellular transport and raft association of a group 2
921 HA from influenza virus. Biochem J 465:305-14.
922 38. Wagner R, Gabriel G, Schlesner M, Alex N, Herwig A, Werner O, Klenk HD.
923 2013. Protease activation mutants elicit protective immunity against highly
924 pathogenic avian influenza viruses of subtype H7 in chickens and mice. Emerg
925 Microbes Infect 2:e7.
926 39. Kordyukova LV, Serebryakova MV, Polyansky AA, Kropotkina EA,

927 Alexeevski AV, Veit M, Efremov RG, Filippova IY, Baratova LA. 2011. Linker
928 and/or transmembrane regions of influenza A/Group-1, A/Group-2, and type B
929 virus hemagglutinins are packed differently within trimers. Biochim Biophys
930 Acta 1808:1843-54.
931 40. Wilson IA, Skehel JJ, Wiley DC. 1981. Structure of the haemagglutinin
932 membrane glycoprotein of influenza virus at 3 A resolution. Nature
933 289:366-73.
934 41. Brand CM, Skehel JJ. 1972. Crystalline antigen from the influenza virus
935 envelope. Nat New Biol 238:145-7.
936 42. Benton DJ, Nans A, Calder LJ, Turner J, Neu U, Lin YP, Ketelaars E,
937 Kallewaard NL, Corti D, Lanzavecchia A, Gamblin SJ, Rosenthal PB, Skehel
938 JJ. 2018. Influenza hemagglutinin membrane anchor. Proc Natl Acad Sci U S
939 A 115:10112-10117.
940 43. Mineev KS, Lyukmanova EN, Krabben L, Serebryakova MV, Shulepko MA,
941 Arseniev AS, Kordyukova LV, Veit M. 2013. Structural investigation of
942 influenza virus hemagglutinin membrane-anchoring peptide. Protein Eng Des
943 Sel 26:547-52.
944 44. Tatulian SA, Tamm LK. 2000. Secondary structure, orientation,
945 oligomerization, and lipid interactions of the transmembrane domain of
946 influenza hemagglutinin. Biochemistry 39:496-507.
947 45. Brett K, Kordyukova LV, Serebryakova MV, Mintaev RR, Alexeevski AV, Veit
948 M. 2014. Site-specific S-acylation of influenza virus hemagglutinin: the

location of the acylation site relative to the membrane border is the decisive factor for attachment of stearate. J Biol Chem 289:34978-89.

46. Thiele C, Hannah MJ, Fahrenholz F, Huttner WB. 2000. Cholesterol binds to synaptophysin and is required for biogenesis of synaptic vesicles. Nat Cell Biol 2:42-9.

47. Mintzer EA, Waarts BL, Wilschut J, Bittman R. 2002. Behavior of a photoactivatable analog of cholesterol, 6-photocholesterol, in model membranes. FEBS Lett 510:181-4.

48. Hulce JJ, Cognetta AB, Niphakis MJ, Tully SE, Cravatt BF. 2013. Proteome-wide mapping of cholesterol-interacting proteins in mammalian cells. Nat Methods 10:259-64.

49. Rodriguez-Boulan E, Paskiet KT, Salas PJ, Bard E. 1984. Intracellular transport of influenza virus hemagglutinin to the apical surface of Madin-Darby canine kidney cells. J Cell Biol 98:308-19.

50. Barman S, Ali A, Hui EK, Adhikary L, Nayak DP. 2001. Transport of viral proteins to the apical membranes and interaction of matrix protein with glycoproteins in the assembly of influenza viruses. Virus Res 77:61-9.

51. Lin S, Naim HY, Rodriguez AC, Roth MG. 1998. Mutations in the middle of the transmembrane domain reverse the polarity of transport of the influenza virus hemagglutinin in MDCK epithelial cells. J Cell Biol 142:51-7.

52. Tall RD, Alonso MA, Roth MG. 2003. Features of influenza HA required for apical sorting differ from those required for association with DRMs or MAL.

971 Traffic 4:838-49.

972 53. Mora R, Rodriguez-Boulan E, Palese P, Garcia-Sastre A. 2002. Apical budding
973 of a recombinant influenza A virus expressing a hemagglutinin protein with a
974 basolateral localization signal. J Virol 76:3544-53.

975 54. Jin H, Leser GP, Zhang J, Lamb RA. 1997. Influenza virus hemagglutinin and
976 neuraminidase cytoplasmic tails control particle shape. EMBO J 16:1236-47.

977 55. Daniels RS, Downie JC, Hay AJ, Knossow M, Skehel JJ, Wang ML, Wiley
978 DC. 1985. Fusion mutants of the influenza virus hemagglutinin glycoprotein.
979 Cell 40:431-9.

980 56. Domanska MK, Wrona D, Kasson PM. 2013. Multiphasic effects of
981 cholesterol on influenza fusion kinetics reflect multiple mechanistic roles.
982 Biophys J 105:1383-7.

983 57. Zawada KE, Wrona D, Rawle RJ, Kasson PM. 2016. Influenza viral
984 membrane fusion is sensitive to sterol concentration but surprisingly robust to
985 sterol chemical identity. Sci Rep 6:29842.

986 58. van Meer G, Voelker DR, Feigenson GW. 2008. Membrane lipids: where they
987 are and how they behave. Nat Rev Mol Cell Biol 9:112-24.

988 59. Wilson RL, Frisz JF, Klitzing HA, Zimmerberg J, Weber PK, Kraft ML. 2015.
989 Hemagglutinin clusters in the plasma membrane are not enriched with
990 cholesterol and sphingolipids. Biophys J 108:1652-1659.

991 60. Siche S, Brett K, Moller L, Kordyukova LV, Mintaev RR, Alexeevski AV, Veit
992 M. 2015. Two Cytoplasmic Acylation Sites and an Adjacent Hydrophobic

Residue, but No Other Conserved Amino Acids in the Cytoplasmic Tail of HA from Influenza A Virus Are Crucial for Virus Replication. Viruses 7:6458-75.

61. Brugger B, Glass B, Haberkant P, Leibrecht I, Wieland FT, Krausslich HG. 2006. The HIV lipidome: a raft with an unusual composition. Proc Natl Acad Sci U S A 103:2641-6.

62. Harris A, Cardone G, Winkler DC, Heymann JB, Brecher M, White JM, Steven AC. 2006. Influenza virus pleiomorphy characterized by cryoelectron tomography. Proc Natl Acad Sci U S A 103:19123-7.

63. Moules V, Terrier O, Yver M, Riteau B, Moriscot C, Ferraris O, Julien T, Giudice E, Rolland JP, Erny A, Bouscambert-Duchamp M, Frobert E, Rosa-Calatrava M, Pu Lin Y, Hay A, Thomas D, Schoehn G, Lina B. 2011. Importance of viral genomic composition in modulating glycoprotein content on the surface of influenza virus particles. Virology 414:51-62.

64. Anderson RG, Jacobson K. 2002. A role for lipid shells in targeting proteins to caveolae, rafts, and other lipid domains. Science 296:1821-5.

65. Jacobson K, Mouritsen OG, Anderson RG. 2007. Lipid rafts: at a crossroad between cell biology and physics. Nat Cell Biol 9:7-14.

66. Vahey MD, Fletcher DA. 2019. Low-Fidelity Assembly of Influenza A Virus Promotes Escape from Host Cells. Cell 176:281-294 e19.

67. Chen BJ, Takeda M, Lamb RA. 2005. Influenza virus hemagglutinin (H3 subtype) requires palmitoylation of its cytoplasmic tail for assembly: M1 proteins of two subtypes differ in their ability to support assembly. J Virol

79:13673-84.

68. Veit M, Kretzschmar E, Kuroda K, Garten W, Schmidt MF, Klenk HD, Rott R. 1991. Site-specific mutagenesis identifies three cysteine residues in the cytoplasmic tail as acylation sites of influenza virus hemagglutinin. J Virol 65:2491-500.

69. Chlanda P, Mekhedov E, Waters H, Sodt A, Schwartz C, Nair V, Blank PS, Zimmerberg J. 2017. Palmitoylation Contributes to Membrane Curvature in Influenza A Virus Assembly and Hemagglutinin-Mediated Membrane Fusion. J Virol 91.

70. Calder LJ, Rosenthal PB. 2016. Cryomicroscopy provides structural snapshots of influenza virus membrane fusion. Nat Struct Mol Biol 23:853-8.

71. Gui L, Ebner JL, Mileant A, Williams JA, Lee KK. 2016. Visualization and Sequencing of Membrane Remodeling Leading to Influenza Virus Fusion. J Virol 90:6948-6962.

72. Zimmerberg J, Kozlov MM. 2006. How proteins produce cellular membrane curvature. Nat Rev Mol Cell Biol 7:9-19.

## FIGURE LEGENDS

**Figure 1: Cholesterol consensus motif (CCM) in HAs of the phylogenetic group 2**

(A) Conservation of the CCM (amino acids YK…LW) in group 2, but not group 1 HAs. A consensus sequence for each HA subtype was assembled from each HA sequence present in the database (60). The consensus sequence of group 1 (H1, H2, H5, H6, H8, H9, H11, H12, H13, H16 subtypes) and group 2 HAs (H3, H4, H7, H10, H14, H15) was then used for the analysis by the WebLogo 3.3 server http://weblogo.threeplusone.com/create.cgi. The height of the stack indicates the sequence conservation, while the heights of each letter the relative frequency of an amino acid at that position. The start and end of the linker region and the start of the transmembrane region (TMR) are indicated by arrows.

(B) Helical wheel projection (http://lbqp.unb.br/NetWheels/) of the sequence YKDVILW of H7 subtype HA. Amino acids forming the CCM are shown as white squares. Y, K, L are on one side of the helix; W is on the other side and thus must be located on another HA monomer of the trimeric spike to contribute to binding of the same cholesterol molecule, but this arrangement of TMR helices is speculative.

**Figure 2: Photocholesterol labeling of HA wt and HA with mutations in the CCM**

(A) Formula of click-photocholesterol (6'-Azi-25-ethinyl-27-norcholestan-3ß-ol). The functional groups diazirine (blue) and azide (red) are encircled.

(B-D) Labeling of CHO-cells expressing HA wt or HA YKLW4A.

After labeling for 16 hours, cells were exposed to uv-light and lysed with 1% Triton.

10% of the lysate was subjected to SDS-PAGE followed by western-blotting with HA2 specific-antiserum to monitor expression levels of HA (B). 90% of the lysate was immunoprecipitated with the same antiserum, HA-photocholesterol was clicked to Cy3 fluorophore, samples were subjected to reducing SDS-PAGE and the fluorescence in the gel was scanned (C). Quantification: Band intensities of (B) and (C) of this and five other experiments were determined and normalized to HA wt = 100%. The mean (58%) ± standard deviation (±13%) is shown (D).

(E-G) Labeling of immunoprecipitated HA wt or HA YKLW4A.

24 hours after transfection CHO cells expressing HA wt or HA YKLW4A were lysed. 10% of the lysate was subjected to SDS-PAGE followed by western-blotting (E). 90% of the lysate was immunoprecipitated, washed antibody-HA complexes were incubated with photochlesterol, uv-irradiated and clicked to Cy3 fluorophore prior to reducing SDS-PAGE and fluorescence scanning (F). Quantification: Band intensities of (E) and (F) of this and three other experiments were determined and normalized to HA wt = 100%. The mean (38%) ± standard deviation (±5%) is shown (G). The asterisks indicate statistically significant differences (****$P < 0.0001$) between wt and the mutant according to a Student's t-test. Mock: untransfected cells. kDa: Molecular weight markers. HA YKLW4A was in each experiment (B-E) expressed at higher levels as HA wt.

(H+I) Labeling of CHO-cells expressing HA wt, HA LA, HA YK2A and HA LW2A.

Experiment was performed as described in (B) and (C). Quantification: Band intensities of (H)) and (I) of this and two other experiments were determined and

1077 normalized to HA wt = 100%. The mean ± standard deviation is shown (J). HA LA
1078 0.92±0.11, YK2A 0.99±0.30 and LW2A 0.97±0.34 relative to HA wt.
1079
1080 **Fig. 3: Effect of mutations in the CCM on virus replication**
1081 (A+B) Growth curves of FPV* wt and FPV* with the indicated mutations in the CCM
1082 of HA. MDCK II cells were infected with virus at an m.o.i. of 0.0005. Culture
1083 supernatants were harvested at the indicated times and tested with HA-assay (A) or
1084 TCID50 (B). Experiments were carried out in triplicate and are displayed as
1085 means±standard deviation. Asterisk indicate statistically significant differences (*P <
1086 0.05, **P < 0.01) between wt and the mutant LW2A according to a Student's t-test.
1087 (C) Competitive growth of FPV* wt and FPV* mutants. Sequencing chromatograms
1088 of cDNA of wild-type and mutant FPV*. MDCK II cells were infected (total moi:
1089 0.0005) with FPV* wt and FPV* YK2A (left) or FPV* LW2A (right) mixed at ratio of
1090 1:5. Supernatants were collected before or at the indicated times after infection, the
1091 viral RNA was isolated and subjected to rtPCR and sequencing. The nucleotide
1092 sequences of wt and mutant HA are listed above the chromatogram.
1093
1094 **Fig. 4 Effect of mutations in the CCM on apical virus budding and transport of**
1095 **HA in polarized cells**
1096 (A) Virus budding in polarized MDCK II cells. Polarized MDCK II cells were
1097 infected with viruses at a m.o.i. of 0.001. Culture medium from both the upper (apical)
1098 and lower (baso) chamber was harvested at 8h, 24h, 34h, and 48h post infection and

1099 virus titers were determined by HA-assays. Asterisk indicate statistically significant
1100 differences (*P < 0.05, **P < 0.01) between wt and the mutant LW2A according to a
1101 Student's t-test.
1102 (B) HA mutant LA, YK2A and LW2A transport in MDCK II cells. Polarized MDCK
1103 II cells were infected with the respective viruses at a m.o.i. of 1. 6h post infection,
1104 cells were fixed and stained with anti-HA2 antiserum and anti-ß-catenin antibody
1105 (basolateral marker), followed by secondary antibody coupled to Alexa Fluor 568 (red
1106 for HA) and Alexa Fluor 488 (green for catenin), respectively.
1107 (C) HA mutant YKLW4A transport in polarized MDCK II cells. MDCK II cells were
1108 transfected with HA mutant YKLW4A and HA wt one day after they were seeded into
1109 24 mm transwell filter membranes. 4 days post transfection; cells were fixed and
1110 permeablized, and stained with primary and secondary antibody as described in (B).
1111 Z-sections with 0.5 µm increments from polarized cells are shown in (B) and (C).
1112 Staining of intracellular structures is visible in (C) especially for YKLW4A since the
1113 cells were permeabilized.
1114

1115 **Fig. 5: Effect of mutations in the CCM on HA incorporation into virus particles**
1116 (A+C) Protein composition of FPV* particles purified from embryonated eggs (A)
1117 and MDCK II cells (C). Viruses were purified using a sucrose gradient (20%-60%)
1118 and subjected to non-reducing SDS-PAGE and Coomassie staining. The position of
1119 the major viral proteins is indicated on the right-hand side, and molecular mass
1120 markers (kDa) are shown on the left-hand side.

(B+D) Quantification of the relative protein composition. Density of HA, NP and M1 bands was determined and the HA/NP and HA/M1 ratios were calculated and normalized to wild type. Results from three virus preparations are displayed as means ±standard deviation. Asterisk (*) indicate statistically significant differences (*P < 0.05) between wt and the mutant LW2A according to a Student's t-test.

**Fig. 6: Effect of mutations in the CCM on cholesterol content and virus morphology**

(A) Cholesterol content of FPV* wild-type (wt) and FPV* mutant particles sucrose-purified from MDCK II cells. Dots indicate the cholesterol concentration (µM) divided by the protein concentration (ng/µl) for each of three virus preparations; the horizontal bar is the mean. Viruses prepared from sister cultures and analyzed in parallel are indicated with the same color.

(B) Normalized cholesterol content (wt=100%) of FPV* mutant particles. Asterisk (*) indicate statistically significant differences (*P < 0.05, **P < 0.01) between wt and the mutant YK2A or mutant LW2A according to a Student's t-test.

**Fig. 7: Effect of mutations in the CCM on hemolysis**

(A) pH dependence: FPV* wt and FPV* mutant particles were adjusted to an HA-titer of $2^6$, adsorbed to chicken erythrocytes and pelleted. Samples were adjusted to the indicated pH values and incubated for 60 min at 37°C. Released hemoglobin (OD 405,) is plotted against the virus titer. Results are depicted as means±standard

1143 deviation from three experiments. NC: negative control: Incubation of RBCs without
1144 virus.
1145 (B) time dependence: Hemolysis was initiated with pH 5 treatment and aliquots were
1146 removed after 0.5, 1, 2, 3 and 4 hours. Results are depicted as means±standard
1147 deviation from three experiments.
1148 (C+D): Comparison of hemolytic activity before and after loading of FPV* wt and
1149 FPV* mutant virus particles with cholesterol. Hemolysis was performed after
1150 acidification to pH 5 for 60 min at 37°C with viruses adjusted to an HA-titer of $2^8$. C:
1151 OD measurements of individual experiments with virus before (open symbols) and
1152 after (closed symbols) loading with cholesterol. Viruses prepared from sister cell
1153 cultures, loaded with cholesterol and measured in parallel are indicated with the same
1154 color. Note that in each experiment the hemolytic activity of mutant virus particles
1155 after loading with cholesterol is lower than the corresponding wild type viruses before
1156 cholesterol loading. D: Normalized increase in hemolytic activity relative to untreated
1157 virus particles (=1) from the same virus preparation. Results of three experiments are
1158 shown as mean±standard deviation.
1159

1160 **Fig. 8: Effect of mutations in the CCM on hemifusion**

1161 (A) Fluorescence dequenching assay using erythrocyte ghosts labelled in the
1162 membrane with the self-quenching lipophilic fluorophore R18. FPV* wt and mutant
1163 viruses were adjusted to an HA-titer of $2^{10}$, adsorbed to R18-labeled ghosts and the
1164 fusion reaction was started by adjusting the pH to 5. The graph shows the mean of

four experiments with two virus preparations. Relative fluorescence dequenching (FDQ, dequenching with Triton-X-100 = 100%) is plotted against the time (min).

(B) Relative extent of fusion (FDQ after 10 min and normalized to wt =100%) is shown as the mean±standard deviation of the four experiments. Asterisk indicate statistically significant differences (*P < 0.05, **P < 0.01, ***P < 0.001) between wt and the mutants according to a Student's t-test. Fitting the curves revealed also a delay in the half time for fusion for the double mutants. The following data were calculated: wt=0.59±0.05 min, LA=0.6±0.1; YK2A= 0.9±0.18; LW2A=0.95±0.1.

**Fig. 9: Effect of complete exchange of the CCM on fusion of cells to erythrocytes**

Fusion of CHO cells expressing HA YKLW4A or HA wt with erythrocytes labeled with the lipid marker R18 and the content marker calcein. 24 hours after transfection cells were treated with trypsin to cleave HA and incubated with double-labelled erythrocytes. Unbound erythrocytes were washed off and cells were treated for 5 min with pH 5, neutralized and monitored with a fluorescence microscope in the calcein channel and R18 channel.

(A) Fluorescence microscopy (40x magnification) show diffusion of calcein (green) into the cytoplasm and of R18 (red) into the plasma membrane of cells expressing HA YKLW4A. Mock: untransfected cells do not show tight binding of erythrocytes to cells.

(B) Comparison of the number of fusion events recorded for HA wt and HA YKLW4A at 20x magnification. Note that the number of erythrocytes is roughly the

same in both microscopic fields, but cells expressing HA YKLW4A exhibit less hemifusion or full fusion.

(C) Three examples of cells expressing HA YKLW4A that exhibit after acidification binding of erythrocytes that neither underwent hemifusion (diffusion of red dye into the plasma membrane) nor full fusion (diffusion of green dye into the cell´s interior, not displayed).

(D) Relative quantification of individual fusion events for cells expressing HA wt or HA YKLW4A. In three transfections at least 100 cells with at least two bound erythrocytes were selected and (based on the result in the fluorescence channel) grouped into one of three categories, either unfused (=binding), hemifused or fully fused to erythrocytes. The total number of counted cells was normalized (=100%) and the percentage of events in each category was calculated and is displayed as the mean ±standard deviation.

A

Group 1 HA

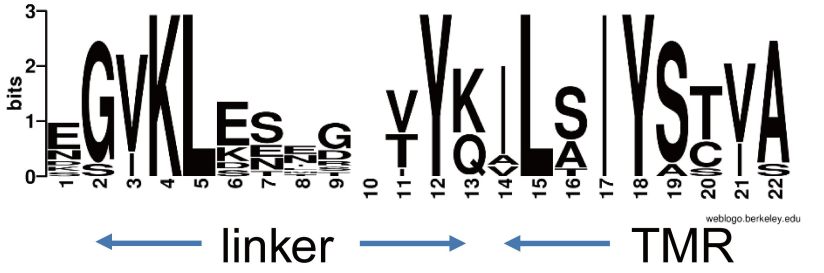


linker TMR

Group 2 HA

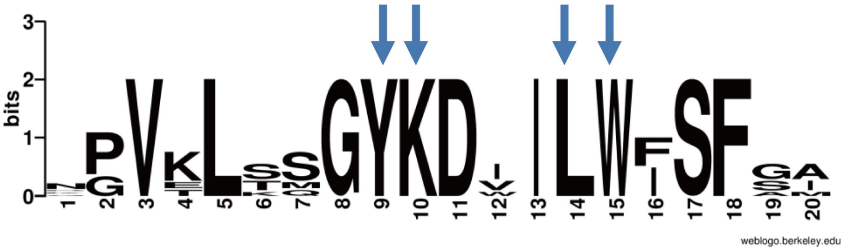


linker TMR

B

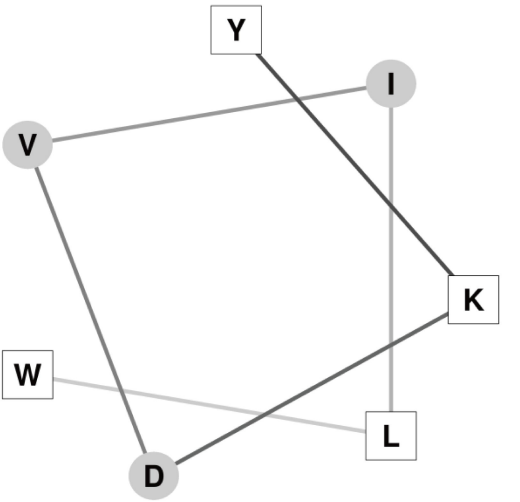

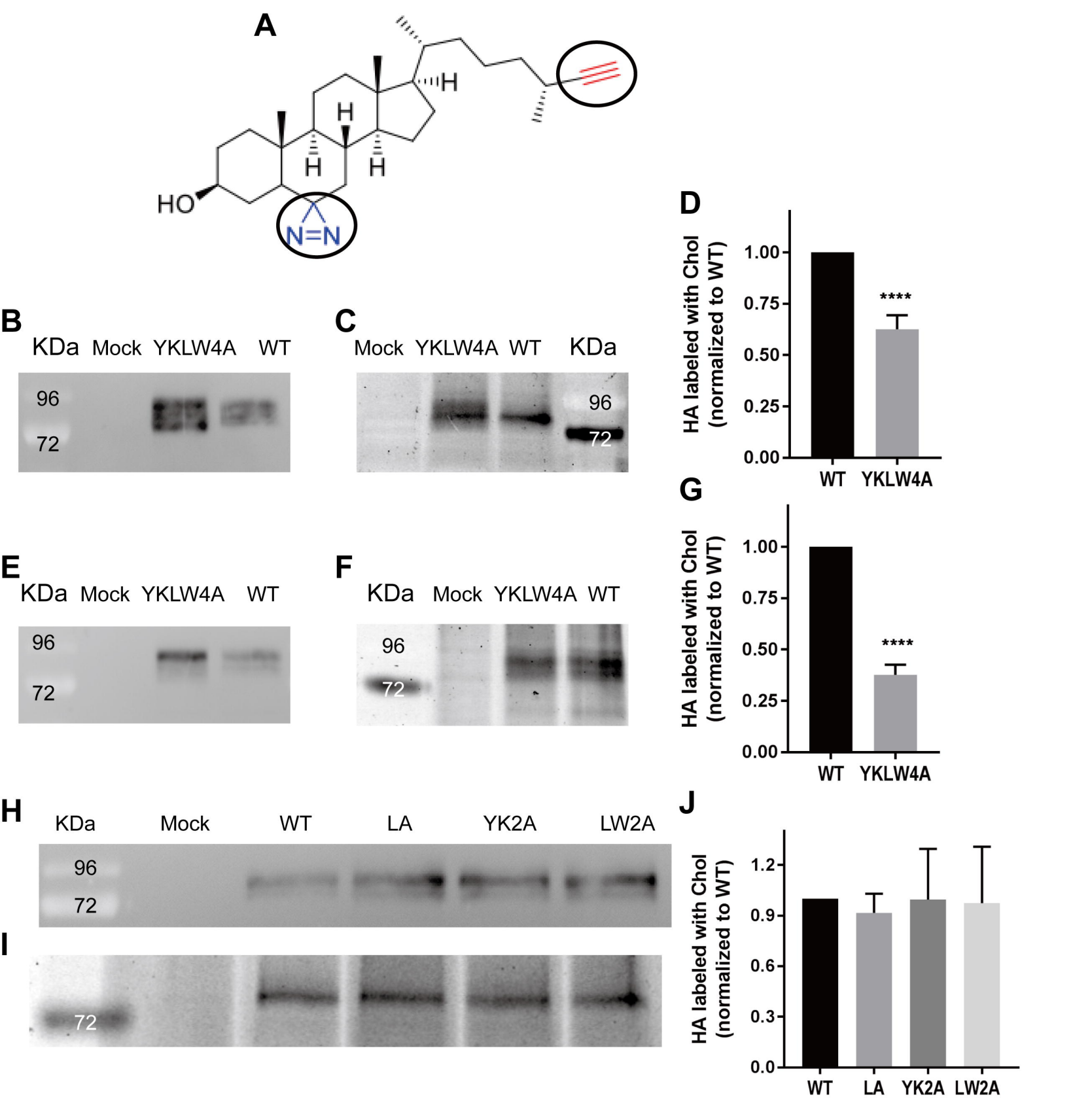
A
HO
N=N
H
H
H
H
B
KDa
Mock
YKLW4A
WT
96
72
C
Mock
YKLW4A
WT
KDa
96
72
D
HA labeled with Chol (normalized to WT)
1.00
0.75
0.50
0.25
0.00
****
WT
YKLW4A
E
KDa
Mock
YKLW4A
WT
96
72
F
KDa
Mock
YKLW4A
WT
96
72
G
HA labeled with Chol (normalized to WT)
1.00
0.75
0.50
0.25
0.00
****
WT
YKLW4A
H
KDa
Mock
WT
LA
YK2A
LW2A
96
72
I
72
J
HA labeled with Chol (normalized to WT)
1.2
0.9
0.6
0.3
0.0
WT
LA
YK2A
LW2A

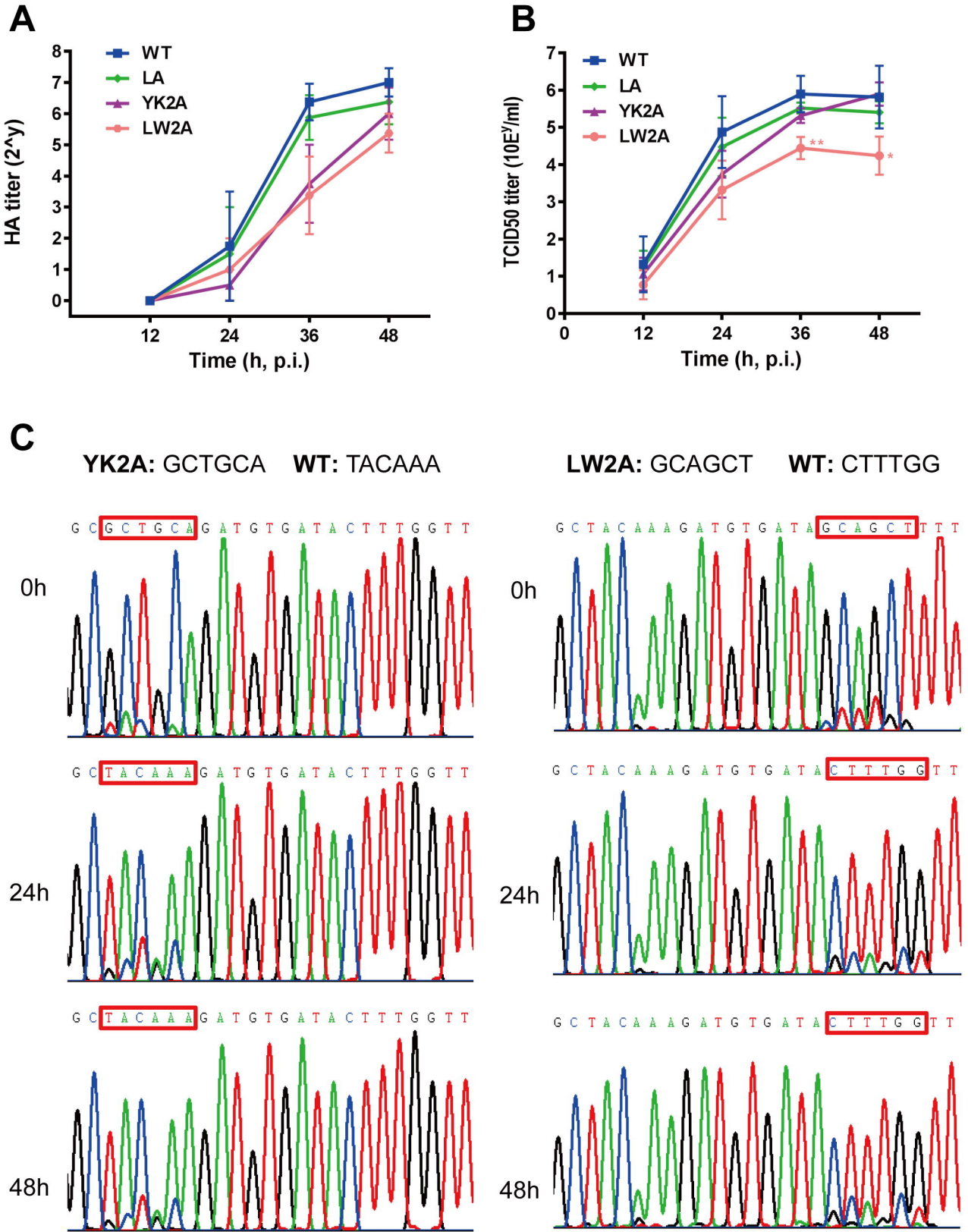
A
HA titer (2^y)
WT
LA
YK2A
LW2A
Time (h, p.i.)
B
TCID50 titer (10E^y/ml)
WT
LA
YK2A
LW2A
Time (h, p.i.)
C
YK2A: GCTGCA WT: TACAAA
LW2A: GCAGCT WT: CTTTGG
0h
24h
48h
0h
24h
48h

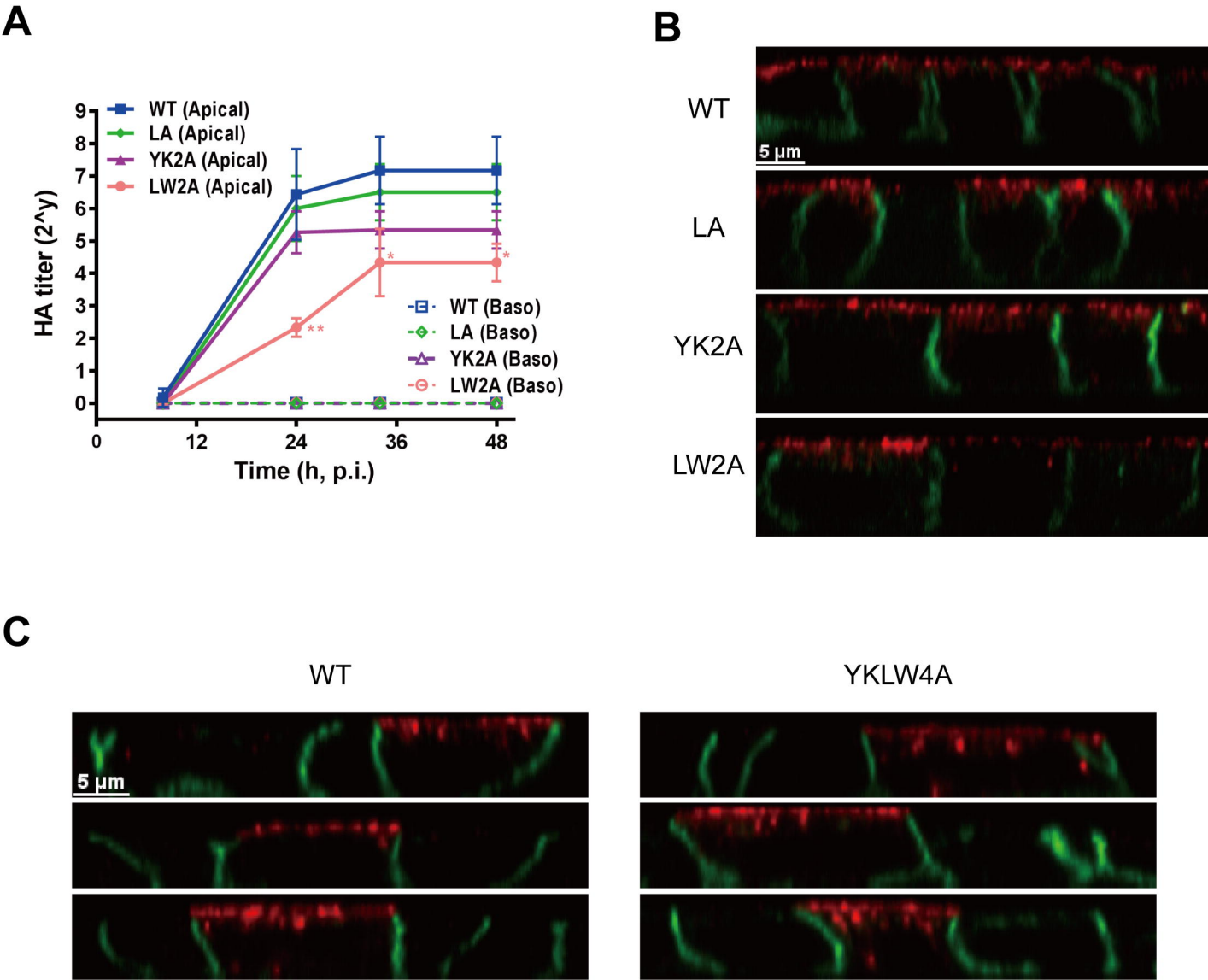
A
WT (Apical)
LA (Apical)
YK2A (Apical)
LW2A (Apical)
WT (Baso)
LA (Baso)
YK2A (Baso)
LW2A (Baso)
HA titer (2^y)
Time (h, p.i.)
0
12
24
36
48
B
WT
LA
YK2A
LW2A
5 μm
C
WT
YKLW4A
5 μm

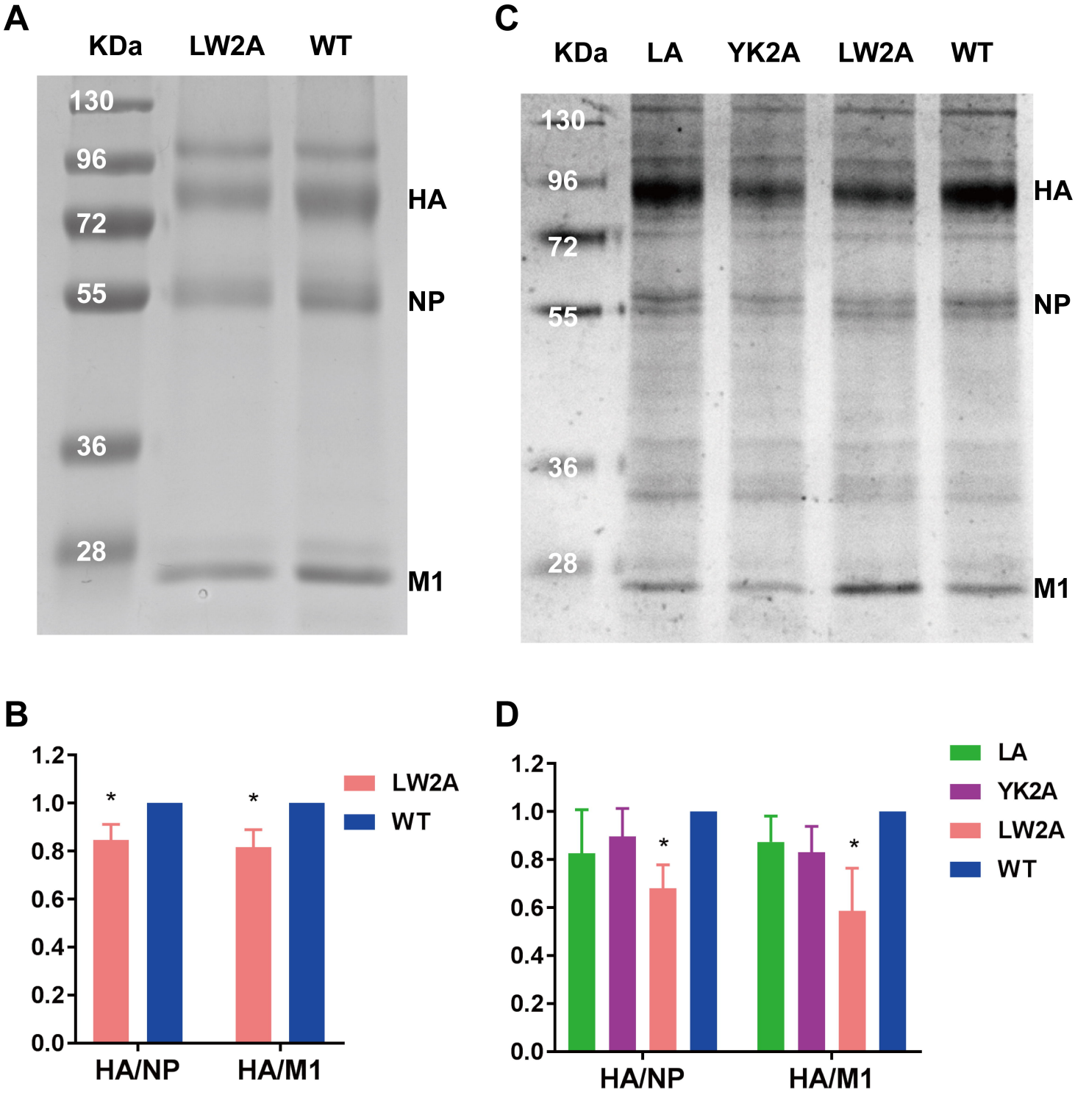
A
KDa
LW2A
WT
130
96
72
55
36
28
HA
NP
M1
C
KDa
LA
YK2A
LW2A
WT
130
96
72
55
36
28
HA
NP
M1
B
1.2
1.0
0.8
0.6
0.4
0.2
0.0
*
*
LW2A
WT
HA/NP
HA/M1
D
1.2
1.0
0.8
0.6
0.4
0.2
0.0
*
*
LA
YK2A
LW2A
WT
HA/NP
HA/M1

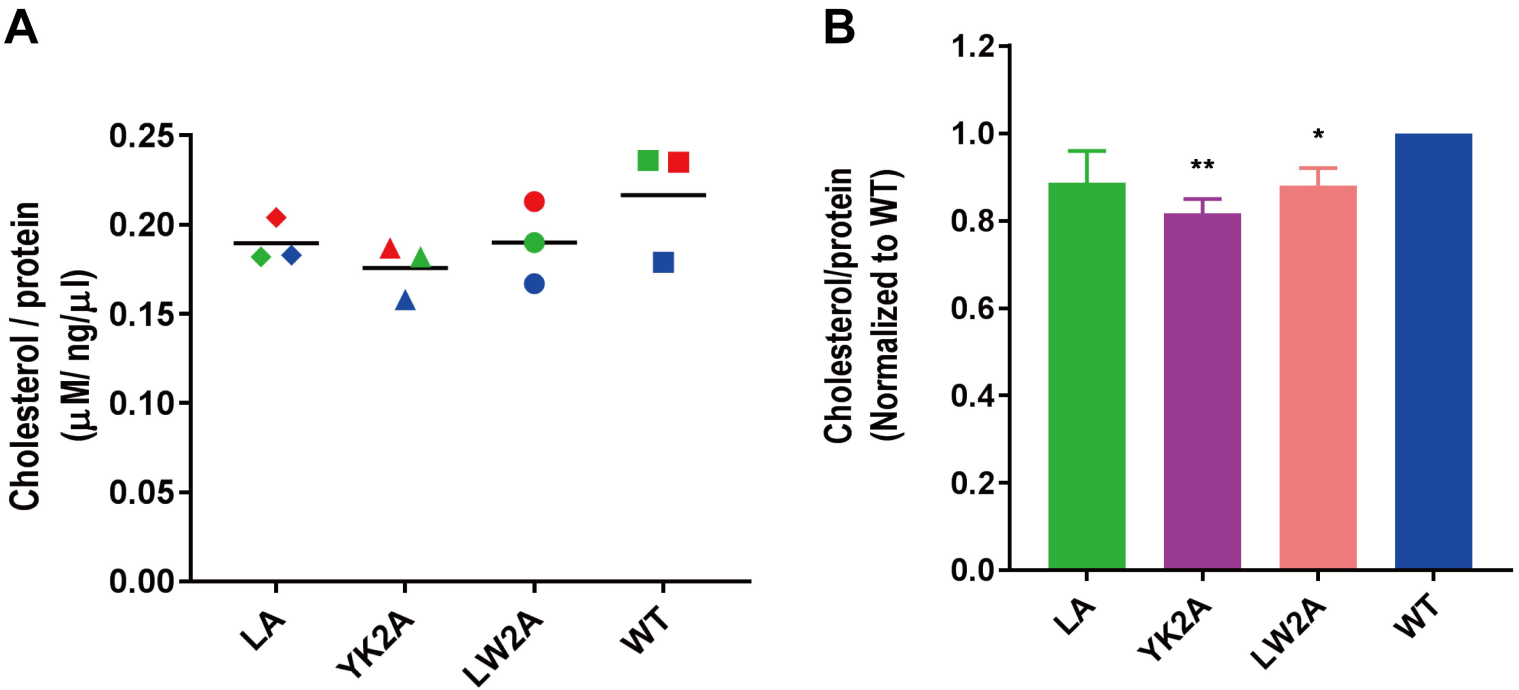
A
Cholesterol / protein
(μM/ ng/μl)
0.25
0.20
0.15
0.10
0.05
0.00
LA
YK2A
LW2A
WT
B
Cholesterol/protein
(Normalized to WT)
1.2
1.0
0.8
0.6
0.4
0.2
0.0
**
*
LA
YK2A
LW2A
WT

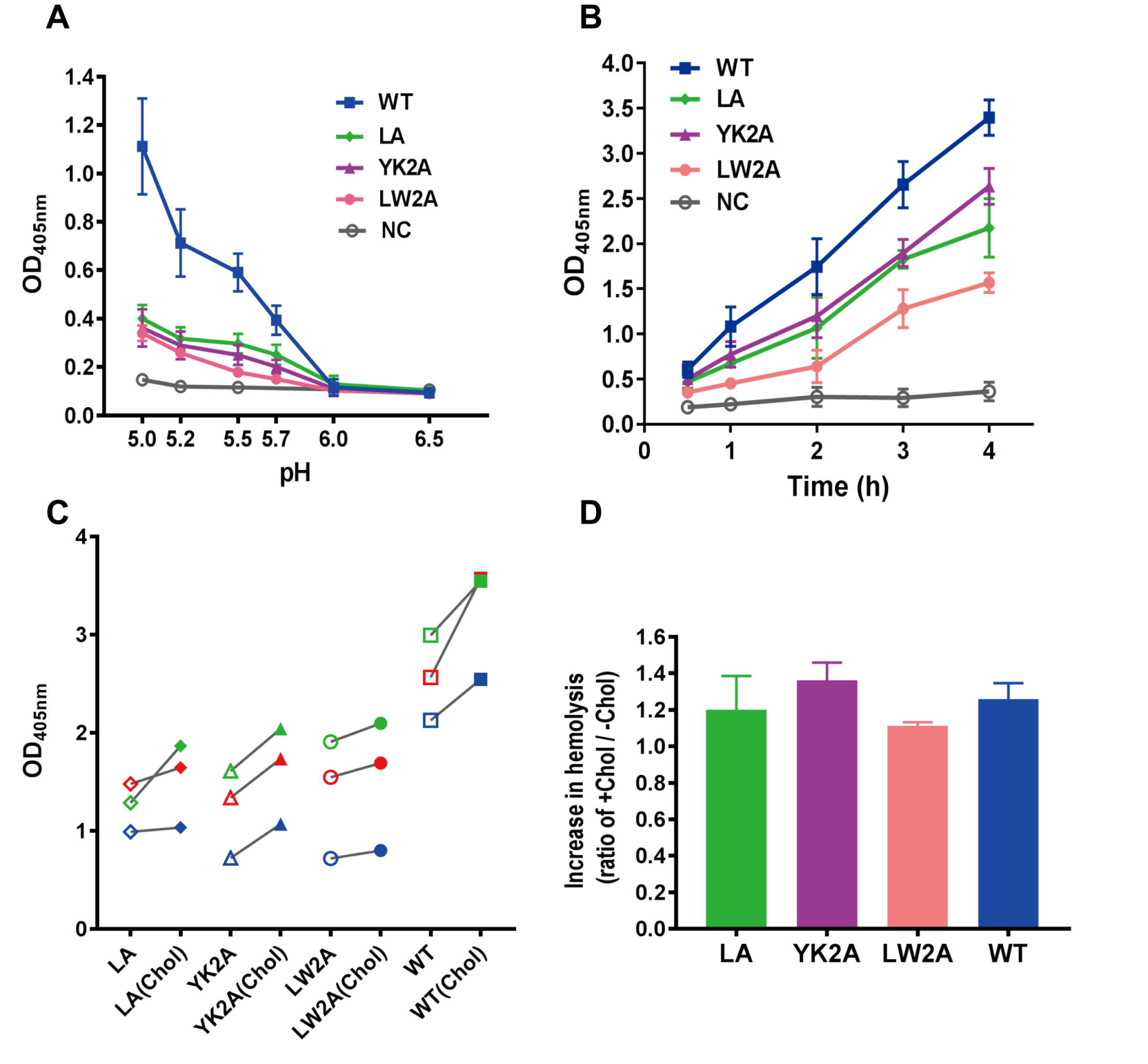
A
B
C
D
WT
LA
YK2A
LW2A
NC
OD405nm
pH
Time (h)
Increase in hemolysis
(ratio of +Chol / -Chol)
LA
LA(Chol)
YK2A
YK2A(Chol)
LW2A
LW2A(Chol)
WT
WT(Chol)

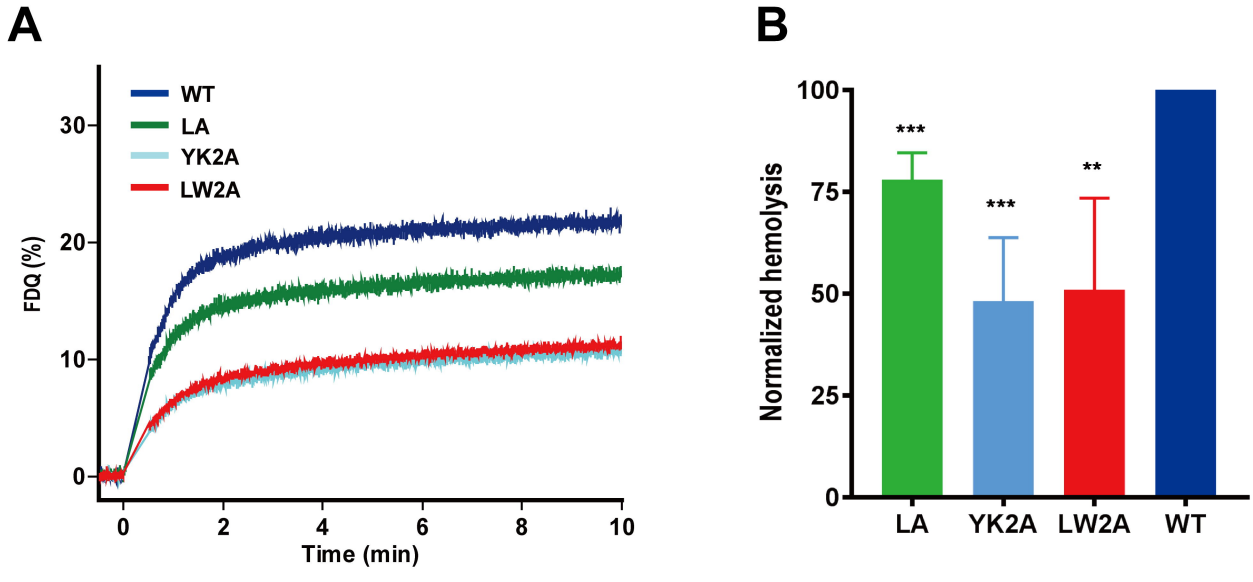
A
WT
LA
YK2A
LW2A
FDQ (%)
30
20
10
0
0
2
4
6
8
10
Time (min)
B
Normalized hemolysis
100
75
50
25
0
***
***
**
LA
YK2A
LW2A
WT

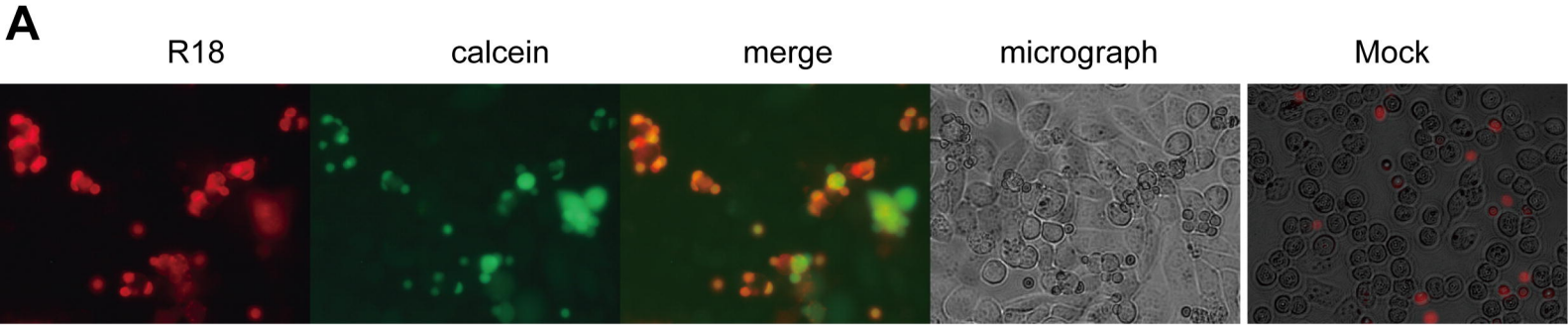
A
R18
calcein
merge
micrograph
Mock

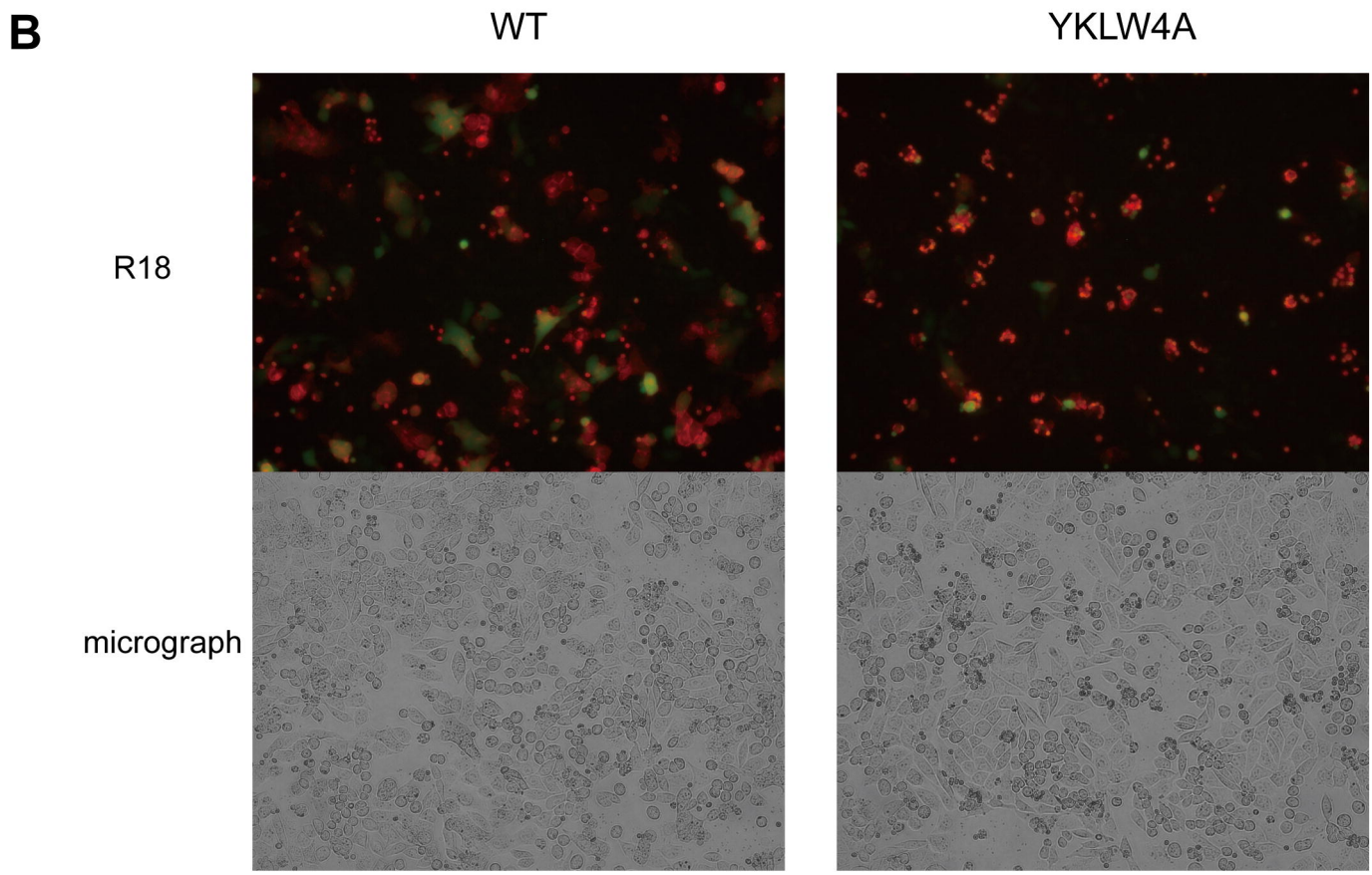
B
WT
YKLW4A
R18
micrograph

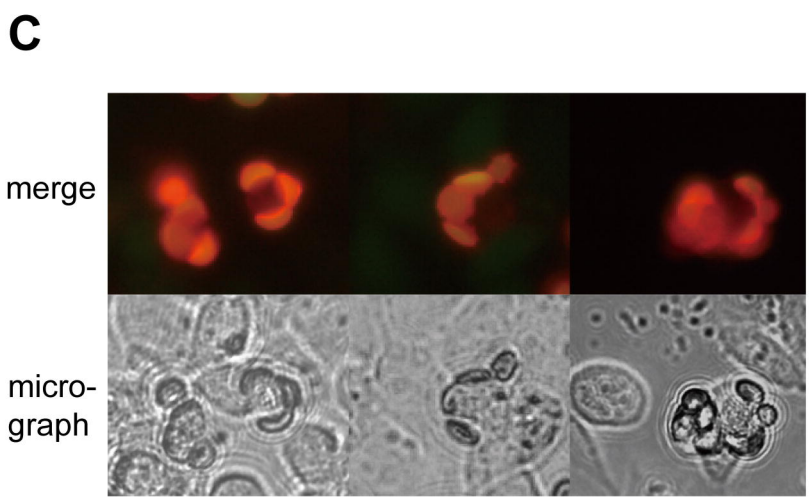
C
merge
micro-
graph

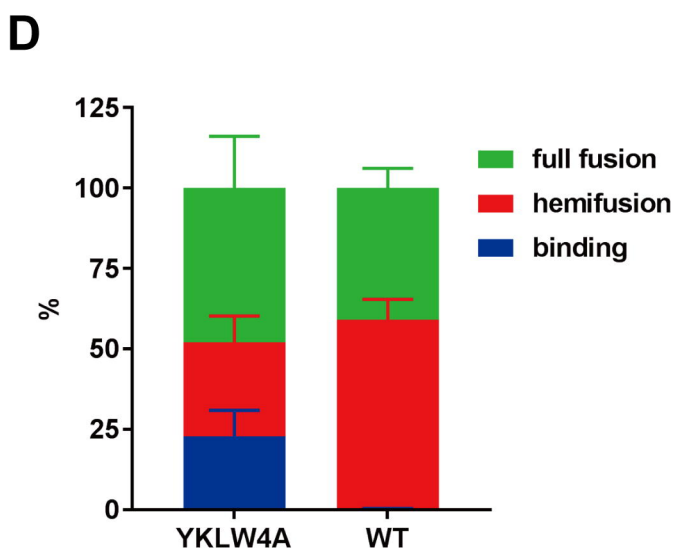
D
125
100
75
50
25
0
%
YKLW4A
WT
full fusion
hemifusion
binding